NOTE TO USERS

Analysis and Testing of MEMS Structures Subjected to Random Environment

Jianliang Ge

A Thesis

in

The Department

of

Mechanical and Industrial Engineering

Presented in Partial Fulfillment of the Requirement s
For the Degree of Master of Applied Science (Mechanical Engineering) at
Concordia University
Montreal, Quebec, Canada

November 2004

Your file Votre référence
ISBN: 0-494-04417-9
Our file Notre référence
ISBN: 0-494-04417-9

ABSTRACT

ANALYSIS AND TESTING OF MEMS STRUCTURES SUBJECTED TO RANDOM ENVIRONMENT

Jianliang Ge

In many applications, MEMS structures are subjected to environments that are stochastic in nature. It could be random loading in the case of pressure sensors. On the other hand, due to random vibration of the body in which MEMS devices are attached, they are usually subjected to random base excitation. Therefore, in general MEMS structures are subjected to random environments which may be either random loading or random base excitation. Moreover, as the operating environments of MEMS structures are random, the performance response such as stress, strain, and displacement of the structures are consequently random. In order to explore the dynamic performance of MEMS structures under random environments, the concepts of spectral density function, variance and covariance and the finite element method have to be studied and employed. Random vibration models of multi-degree-of-freedom system and continuous structures have been developed and applied to MEM structures under random loading and base excitation. Experimental results are also conducted on typical MEM structures to verify the analytical model. Moreover, from application point of view the response of a tire pressure due to random pressure fluctuation inside the tire has been studied and a formulation has been proposed to obtain the spectral density function of the tire pressure with respect to the random pavement roughness. The reliability of MEMS structures in random environments has also been addressed briefly.

ACKNOWLEDGEMENTS

The author thanks his thesis supervisors Dr. Ramin Sedaghati and Dr.Muthukumaran Packirisamy for providing him such an interesting research topic and their financial support. During the development of this thesis, Dr. Ramin Sedaghati and Dr. Muthukumaran Packirisamy have given the author their patient guidance and encouragement, here, the author wishes to express his indebtedness to them.

The author acknowledges the help of Mr. Gino Rinaldi in testing.

Last, the author thanks all his family members.

TABLE OF CONTENTS

LIST OF FIGURES

LIST OF TABLES

NOMENCLATURE

σ	Normal Stress	Pa
τ	Shear Stress	Pa
T	Kinetic Energy	J
U	Strain Energy	J
D	Dissipation Energy	J
$[M]$	System Mass Matrix	
$[C]$	System Damping Matrix	
$[K]$	System Stiffness Matrix	
$N(x)$	Shape Function	
$[\phi]$	Mode Shape Matrix	
$\{q\}$	Modal Coordinates	
ξ_j	Damping Ration of j^{th} Mode	
$\{Q\}$	Modal Force	
δ	Variance, and Covariance	
$R_X(\tau)$	Autocorrelation Function	
$R_{X_1X_2}(\tau)$	Cross Correlation Function	
$S_X(\omega)$	Spectral Density Function	
$S_{XY}(\omega)$	Cross Spectral Density Function	
f_s	Spatial Frequency	$cycles/s$

η	Absolute Height of Pavement Profile	m
$W_\eta(f)$	Power Spectral Density of Road Profile	
I	Moment Inertia of Unsprung Mass	$kg \times m^2$
R	Material Strength	Pa
δ_s	Variance of Stress	Pa
μ_s	Mean Stress	Pa
μ_R	Mean Strength of Material	Pa

CHAPTER 1

INTRODUCTION

1.1 Motivation and Problem Statement

MEMS is an acronym that stands for MicroElectroMechanical Systems. MEMS-based pressure sensors, accelerometers, gyroscopes and actuators have tremendous applications in many fields, especially, in automobile and aerospace industries. In most practical applications, MEMS devices are subjected to random vibrations. For instance, the pressure sensor designed to monitor the fluctuation of the pressure inside a automobile's tire is subjected to random pressure loading induced by the stochastic nature of the road surface. Thus, the measurement of tire pressure is a random phenomenon. Similar phenomenon also occurs in combustion pressure sensor which is employed to monitor engine performance.

Practically, all quantities such as acceleration, pressure, velocity and dynamic forces are stochastic in nature and thus the MEMS devices used to measure and sense these quantities are generally subjected to random environments. Also MEMS devices are widely used in aerospace applications for both sensing and actuating purposes. The main applications are the distributed MEMS pressure sensors at the aircraft wings and body and also the distributed actuators at the wings for aerodynamic control. In both cases,

where the microstructures are attached to wings, the MEMS structures are expected to undergo random base excitation, as the aircraft structure is subjected to the random excitation due to stochastic nature of aerodynamic loading. Since MEMS structures are subjected to both random loading and random base excitation, these random processes are treated as random environments in a general sense. In random environments, MEMS performances such as displacement, deformation, strain, and stress are also stochastic due to the nature of the phenomenon. Therefore, as more and more applications of MEMS in future will involve random environments, it becomes important and essential to study the behavior of MEMS structures under random environments. In this thesis, a complete and comprehensive investigation has been conducted to study the behavior of the continuous microstructure under random environments. The reliability of the MEMS structure under random environments is an important issue which has been addressed in this study. An efficient methodology has also been developed to predict the dynamic performance and reliability of MEMS structures under random environment. Experimental study has also been conducted to validate the methodology and simulation results.

1.2 Literature Review

This thesis focuses on dynamic performance of MEMS structures and their reliability in random environments. As a new emerging technology, MEMS (Microelectromechanical System) or MST (Microsystem Technology) will find applications in almost every field of human interest. MEMS is a broad term that encompasses a fairly nebulous group of products. Essentially, MEMS are any products, ranging in size from a micron to a centimeter, that make use of mechanical, electrical, optical and other properties [1].

Initially, MEMS were developed from technologies used in the semiconductor industry for the production of electronic circuits. Less than 10 years after the invention of the integrated circuit, Nathanson [2] used microelectronic fabrication techniques to make the world's first micromechanical device. By the early 1980s, due to massive improvements in processing technologies, micromechanical devices grew in popularity [3]. In the following years, a new industry was born, where electromechanical systems could be realized on micrometer scales. The result was a whole new class of sensors, machines and actuators that performed common tasks on smaller scales that were ideally suited for mass production. MEMS offer great promises for creating cost-effective, miniaturized and robust sensors or actuators. Although MEMS devices come in a wide

variety of applications, the types of structural parts used in them is rather limited. In most of the applications, MEMS devices are designed with some basic parts, such as cantilever beams (single side clamped, double side clamped), plates, springs (often as cantilever beams), hinges, etc [4]. As this thesis aims at developing a prediction method that could be applied to many applications, the MEMS structures are considered as these basic units or their combinations. In order to extend the application of this method to other complicated structures, Finite Element Method (FEM) is used as an analysis tool.

The finite element method is a numerical procedure for analyzing structures and continua. Petyt [5] gives a brief description of finite elements method's application to structural vibration analysis including those of flexural beam and flexural classic thin plate. Gorman [6] analytically provides highly accurate vibration analysis of rectangular plates with the method of Fourier series. However, in reality, the geometry and boundary conditions of the considered structures are not so simple. As a result, the finite element method has to be used to find the static and dynamic performance of the practical structures. Mukhopadhyay [7] has summarized free vibration characteristics of different geometry plates; however no random vibration studies have been conducted. As mentioned before, practically, the excitations to MEMS structure and the response to

such excitations are random processes, and the MEMS structure undergoes random vibration.

The necessary extensions of random vibration have their roots as early as the work of Albert Einstein [8]. The probabilistic theory of mechanical system behavior arose from theoretical investigations of the motion of particles suspended in a fluid, known as Brownian motion. In his doctoral research, Einstein [9] established the first mathematical treatment of Brownian motion with a parabolic partial differential equation. Subsequently, a generation of researchers generalized Einstein's results using the diffusion equation framework. New methods for the characterization of random process including Fourier analysis, autocorrelation functions, and spectral density functions were developed in 1930s. These spectral methods deal directly with the governing equations of motion and may be more practically applied to complex systems than diffusion-equation-based methods [10]. The spectral approach is more predominant today, particularly for the analysis of linear systems. Much of the original development appears in the communications, and mathematics literature [11]. The response of multi-degree-of-freedom system to random excitations is either obtained analytically or numerically based on some assumptions [10,11]. Few papers deal with the response of multi-degree-of-freedom-system accurately and numerically under random excitations. M.W. Bonilha et

al. [12] proposed an approximate description for the spatial response distribution of the bending wave field generated by the random vibration of thin plate-like structural components. Harichandran [13] presented closed-form solutions for random vibration response integrals arising in the analysis of multi-degree-of-freedom systems to stationary nodal and/or support excitations. The closed-form solutions are adopted by Swanson Analysis Systems, Inc.[13]. Furthermore, Harichandran [14] studied the nonlinear response of laminated fiber reinforced plastic plates modeled with finite elements and excited by stochastic loading. As mentioned earlier, MEMS structure is often exposed to random environment. Thus the design and reliability of MEMS structures in random environment is a very challenging problem for designers. In fact, reliability considerations are of primary importance in safety and critical applications, such as, accelerometers for airbag activation [15] and space applications [16]. For these applications, failure can be catastrophic.

Tanner et al.[17] experimentally studied reliability of MEMS devices in a vibration environment. In the experiments, vibration environment had a peak acceleration of 120g and frequency range of 20 to 2000 Hz. The device chosen for the test was a surface-micromachined unpowered microengine. In this test, two vibration related failures and three electrical related failures out of 22 microengines tested were observed.

Brown et al.[18] focused on reliability and fatigue of MEMS devices. Some researchers explored mechanical response and reliability of MEMS structure in shock environment. There are significant reliability concerns regarding Microsystems under shoch loading, specially in automotive, industrial and space applications[19-22].Shock-loaded MEMS can fail in different modes including fracture [23], delamination [24] and stiction [25]. As a first step toward formulating the guidelines for the design of dynamically reliable MEMS structures, Srikar et al.[26] analyzed the mechanical response and formulated failure criteria for a large class of shock-loaded MEMS. The shocks that occur during service are invariably irregular in pulse shape, jagged in spectral characteristics, and varying from one occurrence to another [27].

Srikar et al.[26] modeled such shock environments approximately by a series of simple shocks during laboratory tests. The predictions of the analyses developed by such models were found to be in agreement with the observed mechanical response and reliability of the device.

Using the Finite Element Method, Wagner et al.[28] presented an approach to optimize polysilicon MEMS structures with respect to shock loads. Although a few analytical and experimental studies for the reliability of particular Microsystems exist [29, 30], there is no comprehensive set of guidelines to design dynamically reliable MEMS

structure. As an attempt to solve this problem, the design issues and reliability of capacitive based MEMS inertial sensors in random environment have been addressed.

In aerospace applications such as launching vehicles, random vibration is caused primarily by acoustic noise in the payload fairing, which is in turn induced by external aerodynamic forces due to dynamic pressure and reflection of rocket exhaust from the ground [1]. In microelectromechanical systems, random vibration can induce a number of failure modes, including fretting in microgear trains and breakage of lead-wires in drive electronics.

In automobile applications, Lu Sun [31,32] built models of vehicle suspension systems subjected to stochastic rough pavement surfaces. In his papers, he modeled vehicle tires as springs and road roughness as base excitations. With these models, the deformation of vehicle tires can be obtained. The relationship between the tire pressure and tire deformation can be established based on this approach to compute the spectral density function of tire pressure according to that of the pavement roughness.

Even though, the MEMS structure is frequently used in random environments, the performance characterization of MEMS in such environment has not been given enough attention in recent times. This thesis attempts to predict MEMS dynamic performance accurately and efficiently, and analyze reliability issues in random environments.

1.3 Introduction to MEMS Structures

MEMS promise a tremendous potential for sensing and actuation on a microscale in many fields from DNA sequencing to information and communication systems. A complete microsystem is a complicated system, however, the individual components of a given system have much simpler configuration. Generally, the mechanical structural elements in MEMS, in general are beam, plate, hinges and their combinations.

Typical types of micromechanical structures that are used for different applications are given in the following figures. Figure 1.1 shows a one-side-fixed beam structures while Figure 1.2 shows typical thin plate structure. Free hinge structure is shown in Figure 1.3. Figure 1.4 presents a two-parallel plate structure that could forms a capacitive pressure sensor, accelerometer or gyroscope.

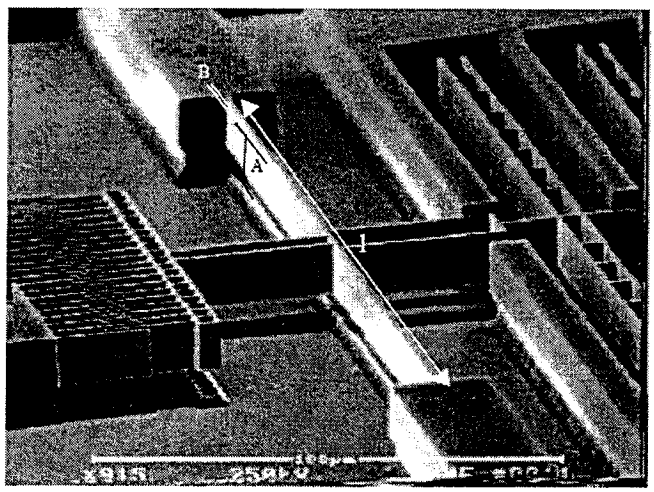

Fig. 1.1: SEM picture of beam with all dimensions labeled [1]

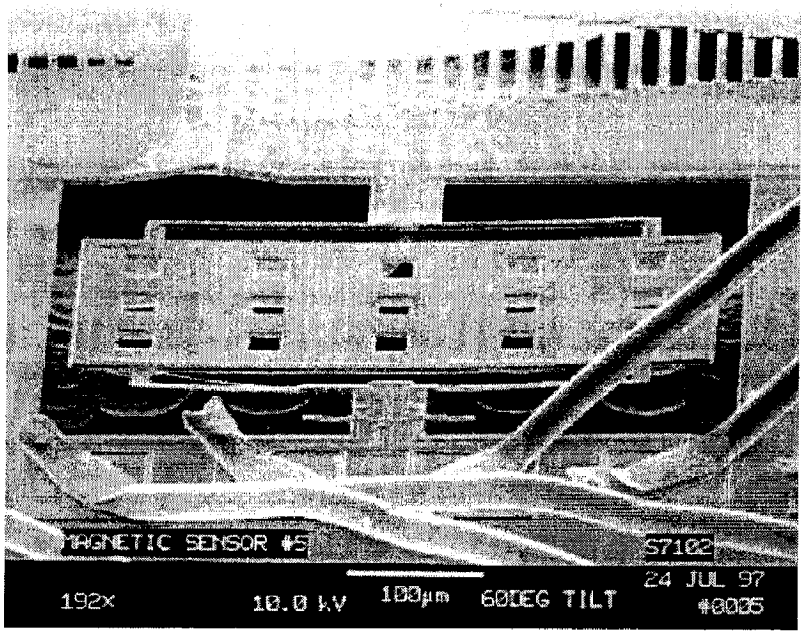

Fig. 1.2: A thin plate viewed at 200X magnification [1]

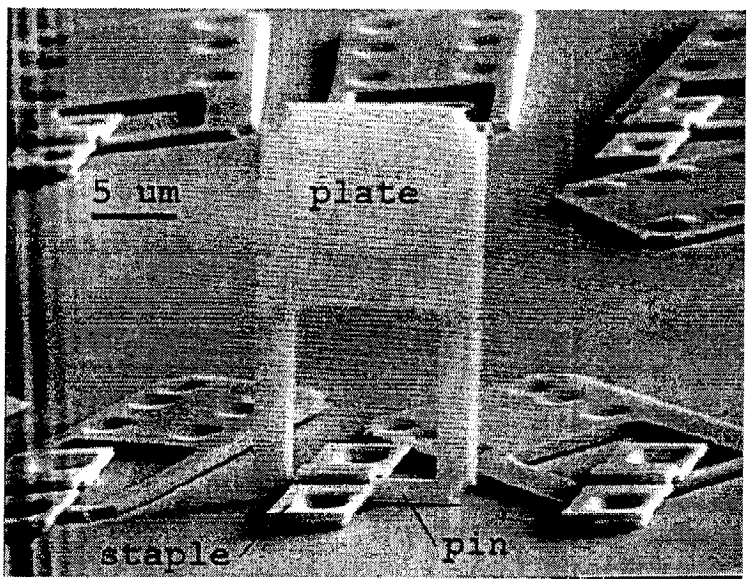

Fig. 1.3: A typical hinge [30]

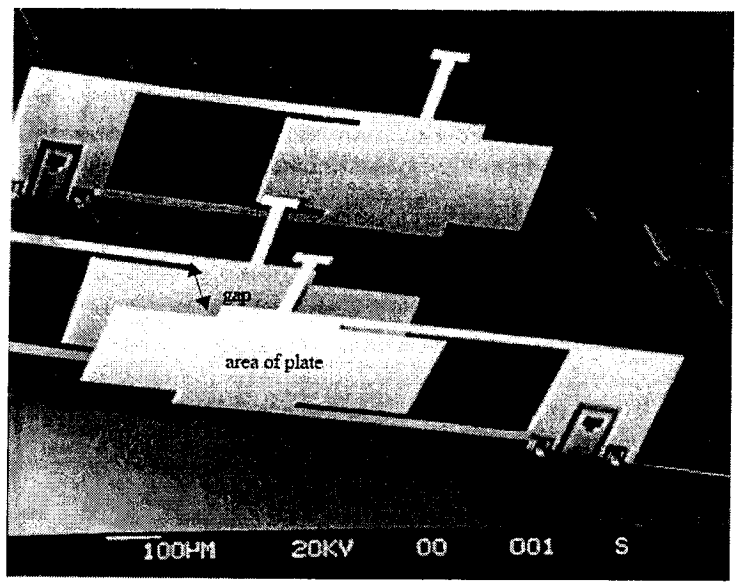

Fig. 1.4: Closeup view of parallel plate capacitor with the area and gap labeled [1]

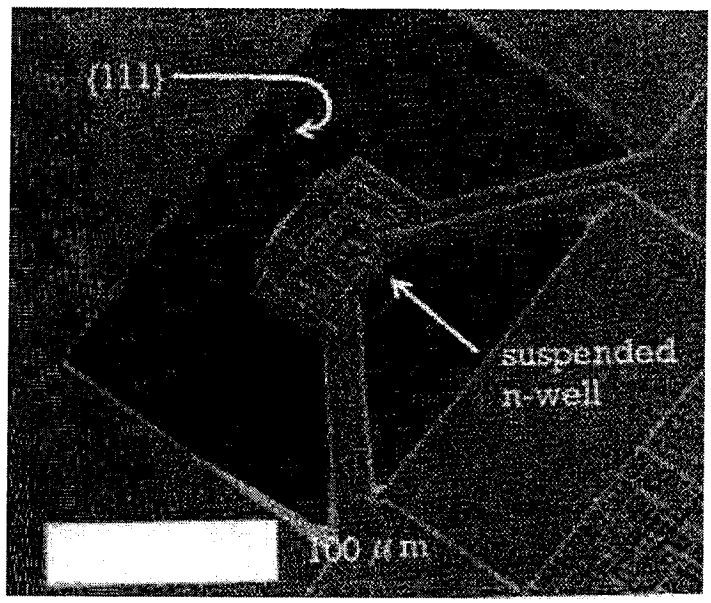

Fig. 1.5: Basic structure of a piezoresistive pressure sensor [34]

Figure 1.5 also shows the basic structure of a piezeresistive pressure sensor. Thus, as it can be realized, the basic structures of MEMS components are beam, plate types of structure, and their combinations. Depending on different situations, the plate can be treated flexible or rigid member. Based on the specific applications, the above MEMS structures can be exposed to stochastic environment.

1.4 Introduction to Random Process

When a MEMS structure operates in random environment, it can be treated as a transfer system. The input of this system is random loading or random base excitation, and the output is the stochastic dynamic performance of the system. Essentially, both output and input are random processes, which are basically the sequence of random variables.

For example, consider the random processes shown in Figures 1.6 and 1.7. The Figures 1.6a and 1.7a show two sample segments of time histories of an excitation from a single random vibration source that occurs in an aerospace vehicle. The acceleration responses that correspond to the individual inputs are shown in Figures 1.6b and 1.7b.

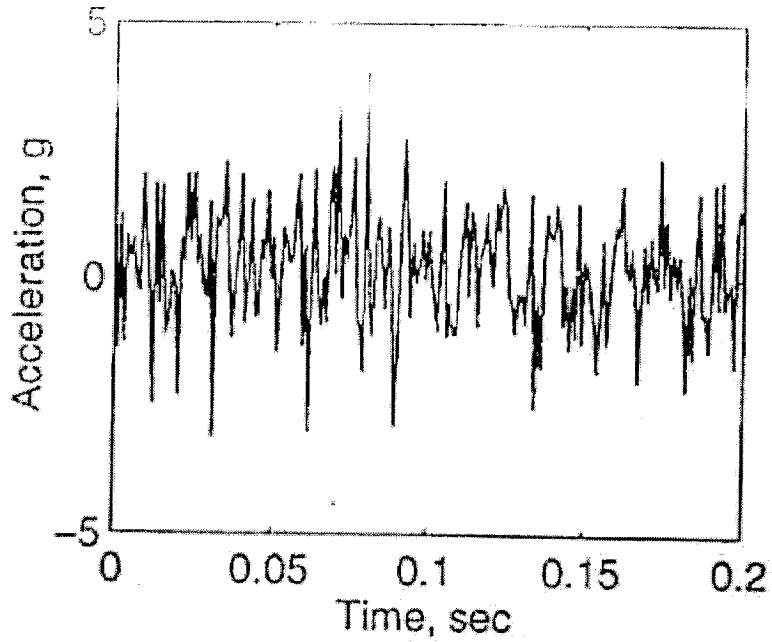

(a)

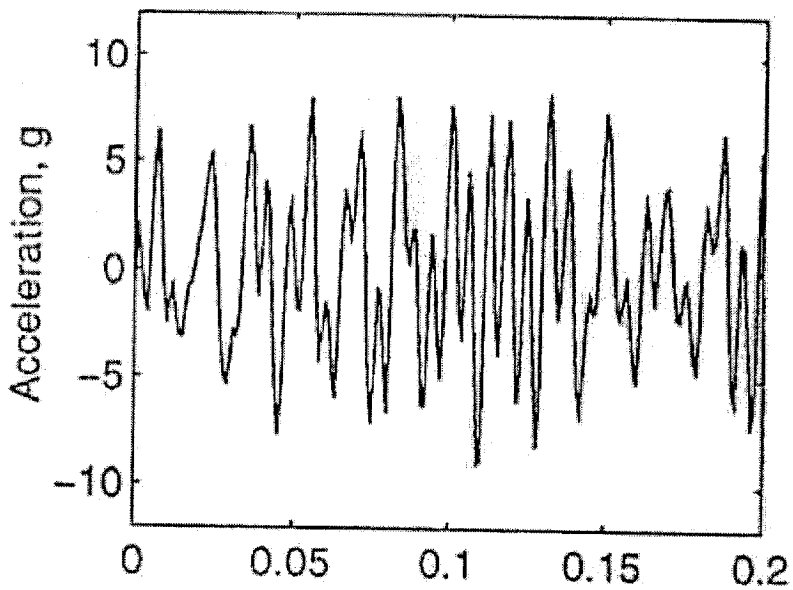

(b)

Fig. 1.6: (a) Segment of random excitation time history from aerospace vehicle
(b) Random vibration response excited by input in part (a) [8]

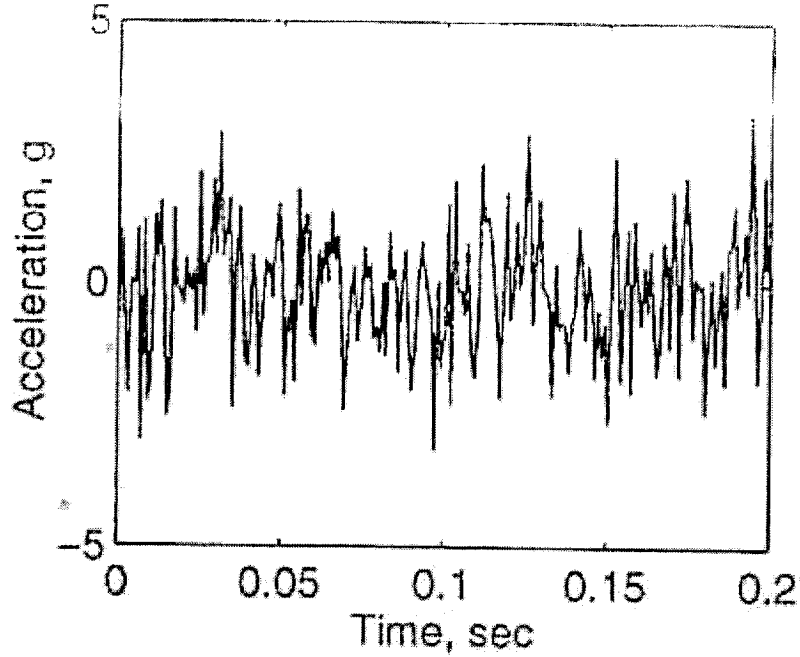

(a)

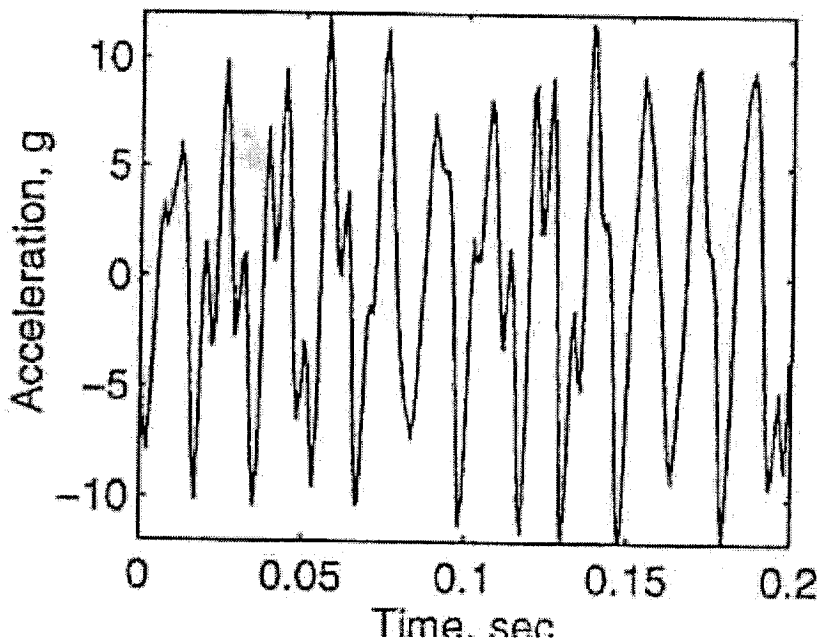

(b)

Fig. 1.7: (a) Segment of random excitation time history measured at same point and same environment. (b) Random vibration response excited by input in part (a) [8]

It is clear that even though the excitations originate from the same nominal sources, they are not identical. Any future excitation and the relative responses will also differ from those measured in the past. It is known that the structural responses to random excitations are random processes.

It is obvious from Figures 1.6 and 1.7 that both excitation and response are not time deterministic. Correlation functions are used to characterize such random processes. In order to study these correlation functions in frequency domain, the random processes are assumed to be stationary in this study. These stationary random processes can be characterized by Spectral Density Function, or SDF, which are Fourier transformations of correlation functions.

1.5 MEMS under Random Environment

Two random environments that will be discussed in this thesis include random base excitations (such as automobile random vibration due to the pavement roughness) and random generalized force (such as uniform random transverse pressure experienced in tire pressure sensors due to the pressure fluctuation)

Automobile vehicles are subjected to random excitation due to pavement roughness and variable velocity. The typical variation of road roughness is shown in Figure 1.8. Such pavement stochastic roughness will lead to random vibration of vehicle

suspension system. As a result, MEMS attached to the vehicle will undergo random base excitation.

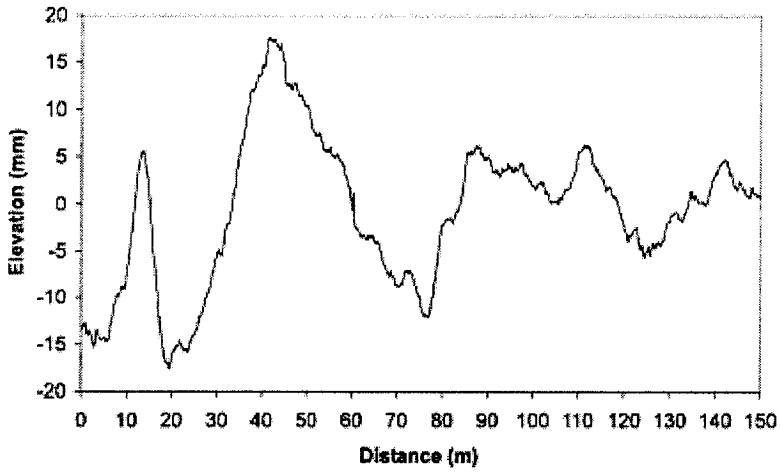

Fig.1. 8: A segment of real pavement roughness [31]

In aerospace, random excitations of MEMS devices can also often occur. For instance, in launch vehicles, the stochastic accelerations are transmitted to MEMS structures or other assemblies. Random vibration input occurs over a broad frequency ranging from about 10 *Hz* to 2000 *Hz*. In the space vehicle launch environment, random vibration is caused by acoustic noise in the payload fairing, which is in turn induced by external aerodynamic forces due to dynamic pressure and reflection of rocket exhaust from the ground.

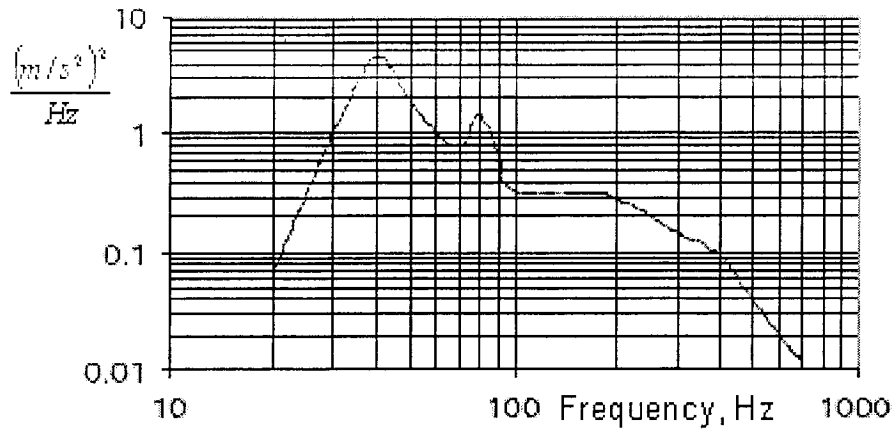

Fig. 1.9: Random vibration levels transmitted to flight article through mounts, the power unit is $(m/s^2)^2/Hz$ [1]

An example of typical random vibration specification realized in flight article is shown in Figure 1.9. The aforementioned random environments are typical base excitation random processes. On the other hand, quantities such as pressure, acceleration, and angular velocity rate which are measured by MEMS sensors are also random in nature. Consequently, MEMS structures endure random forces that can be modeled as generalized uniform spatial stochastic pressure force. In nutshell, the random environments discussed in this paper include stochastic base excitation and stochastic internal loading.

1.6 Present Work

The present thesis constitutes a study regarding the behavior of MEMS structures under random environments. In order to obtain the response of MEMS structure under random environments, the characteristics of MEMS structure and random excitation should be first defined. Based on the Finite Element Method, the thesis presents different models for MEMS structures. The Cross Spectral Density Function of the response has been evaluated analytically and numerically. The equations of motion of the considered MEMS structure have been set up and the input characteristics have been evaluated. The normal mode method is used to develop the differential equations of motion. In most practical problems, the system under random vibration tends to respond globally only in the first few modes. Using normal mode method approximation, the size of the model has been reduced according to the desired frequency range of excitations.

The exact analytical response formulation of multi-degree-of-freedom system without any assumption has been derived. A numerical approach has also been developed and the numerical results are compared with those of analytical solutions. A computer algorithm to compute random response of multi-degree-of-freedom has also been developed.

A dynamic model of continuous structure using Finite Element method has been derived. Applying this model to MEMS structure under random environments, one can predict its performance response. The proposed model has been validated by experimental testing for simple MEMS structures.

A practical application regarding tire pressure sensors has also been investigated. The tire deformation can be obtained if vehicle structure, vehicle velocity, and the road roughness condition are known. Tire pressure fluctuation has also been related to road roughnesses that are characterized by the Spectral Density Function.

Finally, this thesis extends the performance prediction method to analyze design and reliability issues of MEMS in a statistical framework.

1.7 Thesis Organization

This thesis has six chapters. Chapter 1 provided the problem statement and review of the pertinent literature. Introduction to MEMS structure and random process was also discussed in Chapter 1. Chapter 2 will develop finite element formulation for beam and plate type structures. Chapter 3 will focus on different models, and analysis of multi-degree-of-freedom and continuous system in random environment. In this chapter, the analytical and numerical response formulae of multi-degree-of-freedom system will be derived. The finite element model of continuous structures subjected to random base

excitation will be established. Meanwhile, random model of tire pressure will be developed. The application of analysis of continuous structures under random loading will be considered in Chapter 4. In this chapter, the basic information about MEMS will also be summarized. Some typical MEMS structures will be outlined in this chapter. According to different kinds of structures, appropriate models will be set up. MEMS design and reliability problems under random environments will be discussed in this chapter. Chapter 5 will include the experimental setup and experimental results of MEMS structures under random environment. Chapter 6 will conclude with a synthesis of the most important findings and the contribution of the present investigation.

CHAPTER 2

FINITE ELEMENT FORMULATION

2.1 Introduction

The structural components investigated in this thesis are mainly composed of beam and plate elements. Thus it is very important to know the concepts and fundamentals regarding these elements. In this chapter, using Hamilton's principle and Lagrange's equation, the equation of motions have been derived assuming deformation due to shear is negligible. Subsequently, the finite element formulation of the beams and thin plates are presented.

2.2 Elementary Theory of Bending Beams

For a slender beam under bending action as shown in Figure (2.1), the transverse shear and normal stresses are negligible. Moreover, no in-plane shear stress exists if the loads apply in the plane of symmetry.

Considering this, the following relations may be written

$$\sigma_x = E\varepsilon_x,\ \sigma_y = \sigma_z = 0$$
$$\tau_{xy} = \tau_{yz} = \tau_{xz} = 0 \tag{2.1}$$

where σ_x, σ_y and σ_z are the normal stresses along the x (axis of the beam), y and z axis, respectively and τ_{xy}, τ_{yz} and τ_{xz} are shear stresses.

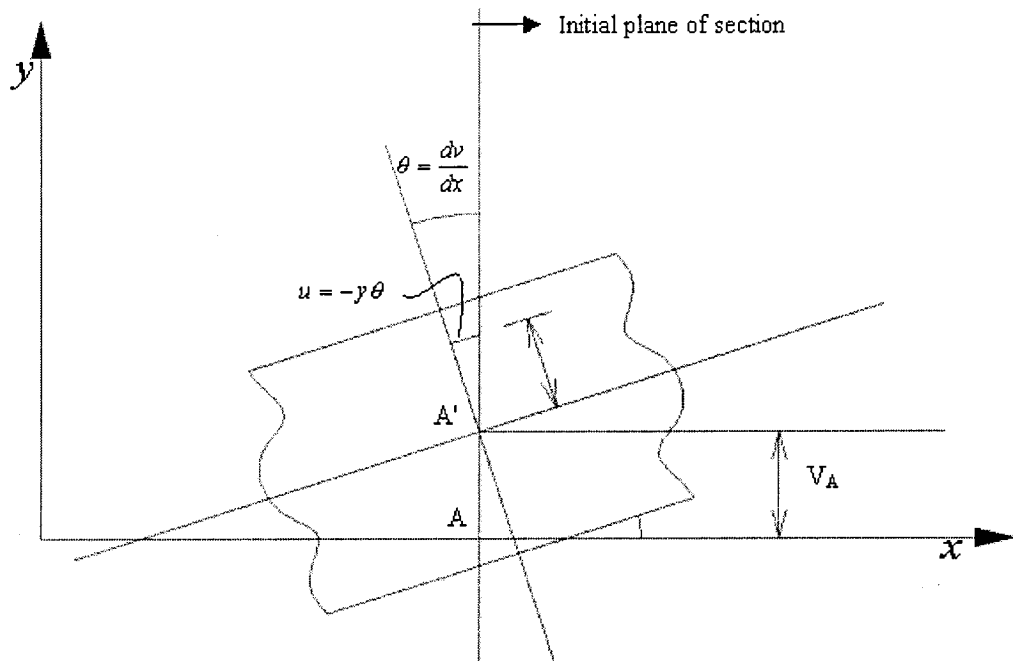

Fig. 2.1 Beam under bending

Considering Eq.(2.1), for a load in plane of $x-y$, it can be concluded that the deflection of the beam v is only a function of x, $v = v(x)$. In other words, all points in a beam at a given longitudinal location x, experience the identical deformation. Axial deformation, u can also be obtained using the relation $\gamma_{xy} = \frac{\partial u}{\partial y} + \frac{\partial v}{\partial x}$, as:

$$u = -y\frac{dv}{dx} + u_0(x) \tag{2.2}$$

where the first part is deformation due to bending action and the second part u_o is the deformation of the center line due to axial loading. Thus, for beam under bending action, Eq. (2.2) may be rewritten as:

$$u = -y\frac{dv}{dx} = -y\theta \tag{2.3}$$

where θ is the slope of the beam axis as shown in the Figure 2.1.

2.3 Theory of Bending Thin Plate

Plates are initially flat structural elements with thicknesses small compared with the remaining dimensions. The thickness of plate is usually divided into equal halves by a plane parallel to the faces. This plane is termed the midsurface of the plate. The plate thickness is measured in a direction normal to the midsurface at each point under consideration. Plates of technical significance are often defined as thin when the ratio of the thickness to the small span length is less than $1/20$.

Assumptions of thin plate are analogous to those associated with the simple bending theory of beams. Therefore, the essence of thin plate is a bi-axial beam. The solution based on this bending theory is therefore approximate. Similar to (2.3), the displacement relationship can be given as,

$$u = -z\frac{\partial w}{\partial x} \qquad v = -z\frac{\partial w}{\partial y} \tag{2.4}$$

Therefore,

$$\varepsilon_x = -z\frac{\partial^2 w}{\partial x^2}, \qquad \varepsilon_y = -z\frac{\partial^2 w}{\partial y^2} \qquad \gamma_{xy} = -2z\frac{\partial^2 w}{\partial x \partial y} \tag{2.5}$$

which provide the strains at any point. The rotation caused on the generic displacements can be described by:

$$\vec{R} = \begin{vmatrix} i & j & k \\ \dfrac{\partial}{\partial x} & \dfrac{\partial}{\partial y} & \dfrac{\partial}{\partial z} \\ u & v & w \end{vmatrix} \tag{2.6}$$

where

$$R_x = \frac{\partial w}{\partial y} \qquad R_y = \frac{\partial w}{\partial x} \qquad R_z = \frac{\partial v}{\partial x} - \frac{\partial u}{\partial y} = -z\left(\frac{\partial^2 w}{\partial x \partial y} - \frac{\partial^2 w}{\partial x \partial y}\right) = 0 \tag{2.7}$$

It is noted that after-mentioned relations are approximate in nature and are based in classic thin beam and plate theory. Hence, they are not the accurate solutions derived from elasticity theory. However, if the beam or plate is thin and deflection is small, the accuracy of the solution would be sufficient for most engineering problems.

2.4 Hamilton's Principle and Lagrange's Equation

The first step in the analysis of any structural vibration problem is the equations of motion. The equations of motion of any dynamic system can be written by using Newton's second law of motion. However, if the structure to be analyzed is a complex system, then the vector addition of all the forces acting at each mass point is difficult. This difficulty may be overcome by the principle of virtual displacements which can be

used to derive the equations of dynamic equilibrium and hence the equations of motions indirectly.

The principle of virtual displacements states that "if a system, which is in equilibrium under the action of a set of forces, is subjected to a virtual displacement, then the total work done by the forces will be zero." Although the principle of virtual displacements alleviate the problem of vector addition of forces, virtual work itself is calculated from the scalar product of two vectors, representing the force and virtual displacement. The disadvantage can be largely overcome by using Hamilton's principle to determine the equations of motion. The Hamilton's principle can be well described as:

$$\int_{t1}^{t2} [\delta(T-U) + \delta W_{nc}]dt = 0 \tag{2.8}$$

where T is potential energy, U is kinetic energy and δW_{nc} is the virtual work of non - conservative forces. This principle can be applied to both discrete and continuous systems.

A discrete or continuous system with n degrees of freedom can be described by n independent generalized displacements $q_1, q_2, \ldots, q_n$. The kinetic energy and strain energy of the system are functions of velocities $\dot{q}_j \ (j = 1,2,\ldots,n)$ and displacements $q_j \ (j = 1,2,\ldots,n)$, respectively. In other words,

$$T = T\left(\dot{q}_1, \dot{q}_2, \ldots, \dot{q}_n\right), \qquad U = U\left(q_1, q_2, \ldots, q_n\right) \tag{2.9}$$

Similarly, the dissipation function is a function of the velocities $\dot{q}_j$, that is

$$D = D\left(\dot{q}_1, \dot{q}_2, \ldots, \dot{q}_n\right) \tag{2.10}$$

Also, the work done by the non-conservative forces can be written in the form:

$$\delta W_{nc} = \sum_{j=1}^{n}\left(Q_j - \frac{\partial D}{\partial \dot{q}_j}\right)\delta q_j \tag{2.11}$$

where the Q_j are generalized forces. Now, consider Eqs. (2.9) and (2.11) and use Hamilton's principle in Eq.(2.8), Lagrange's equations can be obtained as;

$$\frac{d}{dt}\left(\frac{\partial T}{\partial \dot{q}_j}\right) + \frac{\partial D}{\partial \dot{q}_j} + \frac{\partial U}{\partial q_j} = Q_j, \qquad j = 1,2, \ldots, n \tag{2.12}$$

It is noted that the kinetic energy, dissipation function and strain energy can be cast to the following matrix format:

$$\begin{aligned} T &= \frac{1}{2}\left\{\dot{q}\right\}^T [M]\left\{\dot{q}\right\} \\ D &= \frac{1}{2}\left\{\dot{q}\right\}^T [C]\left\{\dot{q}\right\} \\ U &= \frac{1}{2}\{q\}^T [K]\{q\} \end{aligned} \tag{2.13}$$

where $\{q\}$= column vector of system displacements

$\{\dot{q}\}$ =column vector of system velocities

$[M]$ = system mass matrix

$[C]$ = system damping matrix

$[K]$ = system stiffness matrix

Substituting Eq.(2.13) into the Lagrange's equations (2.12) yields the following equations of motion in matrix form:

$$[M]\{\ddot{q}\} + [C]\{\dot{q}\} + [K]\{q\} = \{Q\} \tag{2.14}$$

It can be realized that using Lagrange's equations, one can obtain indirectly the equations of motion using only scalar energy quantities. In the following section, using these principles, the finite element formulation for bending beam and thin plate are derived.

2.5 Finite Element Formulation for Beam Bending Element

In deriving the energy functions for a beam bending element it is assumed that the vibration occurs in one of the principal planes of the beam. Let us consider a beam of length $2a$ and cross-sectional area of A as shown in Figure 2.1. The $xy-$plane is the principal plane in which the beam is vibrating and the $x-$axis coincides with the centroidal axis. Deflection $v = v(x)$ is the displacement of the centroidal axis in the $y-$direction at position x. All parameters such as strains, stresses, potential, and kinetic

energy at any point can be expressed with respect to v. Ignoring the effect of transverse shear deformation, it is assumed that there are two degrees of freedom at each node which are vertical displacement: v and rotation about z axis: $\frac{\partial v}{\partial x}$. Thus each beam element has four degrees of freedom.

To describe the transverse displacement of the beam's centerline with four nodal degrees of freedom, we use a cubic polynomial in natural coordinate as follows:

$$v(\xi) = a_1 + a_2\xi + a_3\xi^2 + a_4\xi^3 \tag{2.15}$$

where $\xi = \frac{x}{a}$. This expression can be written in the following matrix form,

$$v = \begin{bmatrix} 1 & \xi & \xi^2 & \xi^3 \end{bmatrix} \begin{bmatrix} a_1 \\ a_2 \\ a_3 \\ a_4 \end{bmatrix} \tag{2.16}$$

Considering that at $\xi = -1, v = v_1 \; and \; v' = v_1'$, and at $\xi = 1, v = v_2, and \, v' = v_2'$. The displacement function $v(\xi)$ can be expressed as a function of nodal degrees of freedom v_1, v_1', v_2, v_2' as follows:

$$v(\xi) = [N(\xi)]\{v\}_e \tag{2.17}$$

where $[N(\xi)] = [N_1(\xi) \quad aN_2(\xi) \quad N_3(\xi) \quad aN_4(\xi)]$

$$\{v\}_e = \{v_1, v_1', v_2, v_2'\}^T \tag{2.18}$$

and the displacement functions or shape functions are given by

$$N_1(\xi)=\frac{1}{4}(2-3\xi+\xi^2)$$

$$N_2(\xi)=\frac{1}{4}(1-\xi-\xi^2+\xi^3) \tag{2.19}$$

$$N_3(\xi)=\frac{1}{4}(2+3\xi-\xi^3)$$

$$N_4(\xi)=\frac{1}{4}(-1-\xi+\xi^2+\xi^3)$$

Subsequently, the kinetic energy, T_e, potential energy U_e, and virtual work of non-conservative forces, δW_e can be described as:

$$T_e=\frac{1}{2}\int_{-a}^{+a}\rho A\dot{v}^2\,dx \qquad U_e=\frac{1}{2}\int_{-a}^{+a}EI_z(\frac{\partial^2 v}{\partial x^2})^2dx \qquad \delta W_e=\int_{-a}^{+a}p_y\delta v dx \tag{2.20}$$

Substituting the displacement expression formulated in Eq. (2.17) into Eq(2.20) and changing the variable form coordinate x to natural coordinate ξ, we may have the following expressions for kinetic energy.

$$\begin{aligned}T_e&=\frac{1}{2}\int_{-a}^{+a}\rho A\dot{v}^2\,dx=\frac{1}{2}\int_{-1}^{+1}\rho A\dot{v}^2\,ad\xi\\&=\frac{1}{2}\left\{\dot{v}\right\}_e^T\rho Aa\int_{-1}^{-1}[N(\xi)]^T[N(\xi)]d\xi\left\{\dot{v}\right\}_e\end{aligned} \tag{2.21}$$

Thus it can be realized that the element mass matrix is equivalent to:

$$[m]_e=\rho Aa\int_{-1}^{=1}[N(\xi)]^T[N(\xi)]d\xi \tag{2.22}$$

Similarly, the element stiffness matrix may be obtained as

$$[k]_e = \frac{EI_z}{a^3}\int_{-1}^{+1}\left[N''(\xi)\right]^T\left[N''(\xi)\right]d\xi \tag{2.23}$$

Also the element equivalent nodal force vector can be obtained as:

$$\{f\}_e = a\int_{-1}^{+1} p_y[N(\xi)]^T d\xi \tag{2.24}$$

2.6 Element Formulation of a Bending Thin Plate

Flat plate structures are subjected to dynamic loads normal to their plane. This results in flexural vibration. Such structures can be analyzed by dividing the plate into an assemblage of two dimensional finite elements called plate bending elements. These elements may be either triangular, rectangular or quadrilateral in shape. In this section, rectangular element's characteristics based on thin plate theory and Hamilton's principle will be derived.

In general, the strain energy stored in a 3D- element is given by:

$$U_e = \frac{1}{2}\int_v (\sigma_x\varepsilon_x + \sigma_y\varepsilon_y + \sigma_z\varepsilon_z + \tau_{xy}\gamma_{xy} + \tau_{xz}\gamma_{xz} + \tau_{yz}\gamma_{yz})dV \tag{2.25}$$

For 2D- thin plate shown in Figure 2.2, Eq.(2.25) can be simplified as:

$$\begin{aligned} U_e &= \frac{1}{2}\int_V (\sigma_x\varepsilon_x + \sigma_y\varepsilon_y + \tau_{xy}\gamma_{xy})dV \\ &= \frac{1}{2}\int_A \frac{h^3}{12}\{x\}^T[D]\{x\}dA \end{aligned} \tag{2.26}$$

where h is the thickness and

$$\{x\}=\begin{bmatrix}\dfrac{\partial^2 w}{\partial x^2}\\ \dfrac{\partial^2 w}{\partial y^2}\\ 2\dfrac{\partial^2 w}{\partial x\partial y}\end{bmatrix} \qquad [D]=\begin{bmatrix}\dfrac{E}{(1-\nu^2)} & \dfrac{E}{(1-\nu^2)}\nu & 0\\ \dfrac{E}{(1-\nu^2)}\nu & \dfrac{E}{(1-\nu^2)} & 0\\ 0 & 0 & \dfrac{E}{2(1+\nu)}\end{bmatrix}$$

where w is the transverse displacement in the z direction.

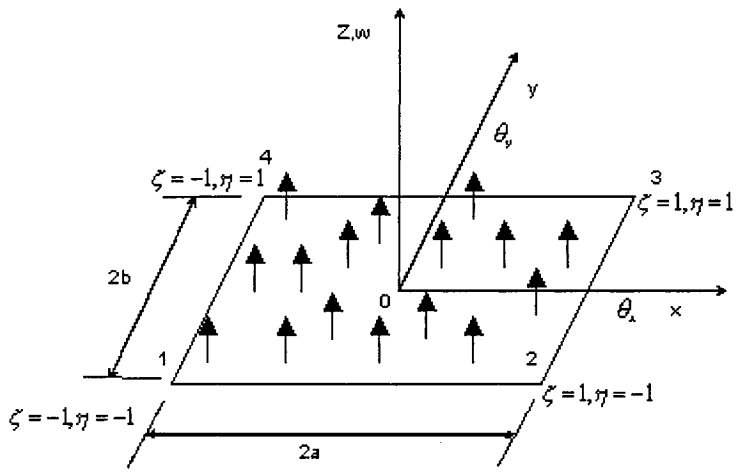

Fig. 2.2 A plate element under transverse loading

It is noted that second derivative of w is presented in the formulation. Thus w and its first derivative should be continuous function for finite element formulation. The displacement function for plate element may be approximated as:

$$w = a_1 + a_2 x + a_3 y + a_4 x^2 + a_5 xy + a_6 y^2 + higher\ order\ forms \qquad (2.27)$$

Rectangular element shown in Figure 2.2 contains 4 nodal points, and each have three degrees of freedom ($w, \dfrac{\partial w}{\partial y}, -\dfrac{\partial w}{\partial x}$).

In terms of the natural coordinates, the three degrees of freedom can be expressed as w, θ_x and θ_y, where

$$\theta_x = \frac{1}{b}\frac{\partial w}{\partial \eta}, \qquad \theta_y = -\frac{1}{a}\frac{\partial w}{\partial \xi} \tag{2.28}$$

in which $\xi = \frac{x}{a}$, $\eta = \frac{y}{b}$

Since the element has twelve degrees of freedom, the displacement function in Equation.(2.27) can be represented by a polynomial having twelve terms, as:

$$w = a_1 + a_2\xi + a_3\eta + a_4\xi^2 + a_5\xi\eta + a_6\eta^2 + a_7\xi^3 + a_8\xi^2\eta + a_9\xi\eta^2 + a_{10}\eta^3 + a_{11}\xi^3\eta + a_{12}\xi\eta^3 \tag{2.29}$$

Similar to the beam element, displacement function can be expressed as a function of nodal degrees of freedom as:

$$\begin{aligned} w &= [N_1(\xi,\eta) \quad N_2(\xi,\eta) \quad N_3(\xi,\eta) \quad N_4(\xi,\eta)]\{w\}_e \\ &= [N(\xi,\eta)]\{w\}_e \end{aligned} \tag{2.30}$$

where, $\{w\}_e$ is the element nodal displacement vector described as:

$$\{w\}_e = \lfloor w_1 \;\; \theta_{x1} \;\; \theta_{y1} \;\; \ldots \;\; w_4 \;\; \theta_{x4} \;\; \theta_{y4} \rfloor \tag{2.31}$$

and $N(\xi,\eta)$ is the shape function which can be expressed as:

$$N_j^T(\xi,\eta) = \begin{bmatrix} \frac{1}{8}(1+\xi_j\xi)(1+\eta_j\eta)(2+\xi_j\xi+\eta_j\eta-\xi^2-\eta^2) \\ \frac{b}{8}(1+\xi_j\xi)(\eta_j+\eta)(\eta^2-1) \\ -\frac{a}{8}(\xi_j+\xi)(\xi^2-1)(1+\eta_j\eta) \end{bmatrix} \tag{2.32}$$

(ξ_j, η_j) is the coordinates of node j.

Substituting displacement function in Eq.(2.30) into kinetic and potential energies, and virtual work expressions, we may have:

$$T_e = \frac{1}{2}\left\{\dot{w}\right\}_e^T [m]_e \left\{\dot{w}\right\}_e$$

where mass matrix $[m]_e$ is

$$\begin{aligned}[m]_e &= \int_{A_e} \rho h [N]^T [N] dA \\ &= \rho h ab \int_{-1}^{+1}\int_{-1}^{+1} [N(\xi,\eta)]^T [N(\xi,\eta)] d\xi d\eta \end{aligned} \tag{2.33}$$

Similarly, using potential energy in Eq.(2.26), we can obtain the element stiffness matrix as;

$$[k]_e = \int_{A_e} \frac{h^3}{12} [B]^T [D][B] dA \tag{2.34}$$

where

$$[B] = \begin{bmatrix} \partial^2/\partial x^2 \\ \partial^2/\partial y^2 \\ 2\partial^2/\partial x \partial y \end{bmatrix} [N] = \begin{bmatrix} \partial^2/(a^2 \partial \xi^2) \\ \partial^2/(b^2 \partial \eta^2) \\ 2\partial^2/(ab \partial \xi \partial \eta) \end{bmatrix} [N(\xi,\eta)]$$

and finally the equivalent nodal force can be expressed as:

$$\{f\}_e = \int_A [N]^T p_z dA \tag{2.35}$$

CHAPTER 3

MODELING AND ANALYSIS OF CONTINUOUS STRUCTURE UNDER RANDOM ENVIRONMENT

In the previous chapter, the element's characteristics such as inertia, stiffness, and the equivalent generalized nodal forces due to external forces have been obtained. This chapter contains: the process to assemble elements into whole structure, normal mode method and size reduction technique, random process and its characteristics in time and frequency domain, derivation of response of multi-degree-of-freedom due to random loading, and the modeling of continuous structure subjected to the random base excitation.

3.1 Characteristics of Continuous Structure

Once the element characteristics are found in a common global coordinate system, the next step is to construct the system equations through the assemblage of the element equations. The procedure for constructing the system motion equations is equivalent to estimate total kinetic energy, potential energy and virtual work done by the external work in terms of global nodal displacements. Such procedure is the same regardless of the type of the problem and the number and type of elements used.

The procedure of assembling the elements characteristics is based on two principles.

1) The kinetic energy, potential energy and virtual work of the whole system are the summation of building blocks (elements).

2) At the nodes where elements are connected, the values of the unknown nodal degrees of freedom are the same for all elements joining at that node (compatibility condition). Thus the system characteristics can be obtained by assembling of the element characteristics:

$$[M]=\sum_{i=1}^{E}[m]_i \qquad [K]=\sum_{i=1}^{E}[k]_i \qquad [F]=\sum_{i=1}^{E}[f]_i \tag{3.1}$$

where $[M],[K],[F]$ are the system mass, and stiffness matrices and nodal force vector. E is the total number of elements and $[m]_i,[k]_i,[f]_i$ are the mass, stiffness, and nodal force vector associated with of i^{th} element respectively. If the structure have N nodal degrees of freedom (including the boundary and restrained degrees of freedom), element characteristics should be expanded to the order of $N\times N, N\times N, N\times 1$ respectively by including zeros in the remaining locations.

3.2 Boundary Conditions

As previously mentioned, the system equations of entire domain can be obtained by assembling the element equations. The final format of the continuous structure discretised into elements may be described by:

$$[M]\{\ddot{X}\}+[C]\{\dot{X}\}+[K]\{X\}=\{F\} \tag{3.2}$$

Equation (3.2) has to be solved for unknown nodal displacement vector with boundary conditions.

There are two types of boundary conditions: forced or geometric or essential and free or natural boundary conditions. Because the motion equations are not derived by direct method, only forced boundary conditions have to be specified and the natural boundary conditions will be implicitly satisfied in the solution procedure.

For example, Figure 3.1 is a cantilever plate subjected to a concentrated load. Side AD is clamped, the degrees of freedom at this side are all zero. On the hand, side AB, BC, and CD are free of any forces, but it is not necessary to describe the boundary conditions since the characteristics of the system are not derived in the direct method. The results obtained will automatically satisfy these boundary conditions.

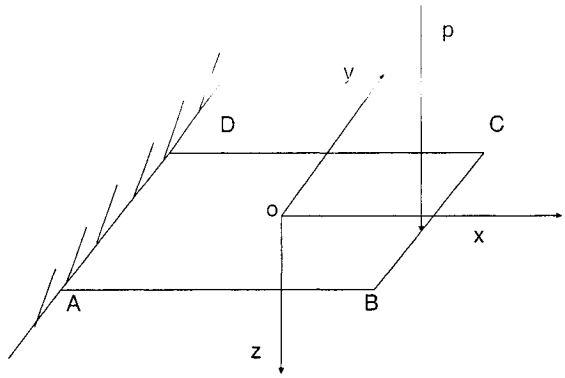

Figure 3.1 A cantilever plate subjected to a concentrated load

3.3 Modal Analysis of Multi-Degree-of-Freedom System

As mentioned before, the equation of motion of a discretised continuous structure can be cast into the form described by Eq.(3.2).

$$[M]\{\ddot{X}\}+[C]\{\dot{X}\}+[K]\{X\}=\{F\} \tag{3.2}$$

which are basically N simultaneous coupled differential equations. In this study, the normal mode method has been employed to decouple the above coupled differential equations by transformation of generalized coordinate to modal coordinate. Since any vector in N-dimensional space can be expressed as a linear combination of N linearly independent vectors, thus it can be written as:

$$\{X\}=[\phi]\{q\} \tag{3.3}$$

where the vector $\{q\}$contains the new coordinates (modal coordinates), and $[\phi]$ is the orthogonal transformation matrix, which consists of normal modes of the system. Substituting (3.3) into Equation (3.2) and pre-multiply both sides by $[\phi]^T$, we may have:

$$\left[\bar{M}\right]\{\ddot{q}\}+\left[\bar{C}\right]\{\dot{q}\}+\left[\bar{K}\right]\{q\}=\{Q\} \tag{3.4}$$

where

$$\left[\bar{M}\right]=[\phi]^T[M][\phi],\ \left[\bar{K}\right]=[\phi]^T[K][\phi],\ \left[\bar{C}\right]=[\phi]^T[C][\phi]\ \text{, and}\ \{Q\}=[\phi]^T\{F\} \tag{3.5}$$

It is noted that the modal mass matrix $\left[\bar{M}\right]$ and modal stiffness matrix $\left[\bar{K}\right]$ stiffness are diagonal matrices. If the damping is proportional to the mass and stiffness (proportional damping), the matrix $\left[\bar{C}\right]$ is also diagonal and equation (3.4) is then completely uncoupled and its i^{th} equation may be written in the following form:

$$\ddot{q}_i+2\xi_i\omega_i\dot{q}_i+\omega_i^2 q_i=\frac{Q_i(t)}{M_i} \tag{3.6}$$

where M_i is the i^{th} modal mass, ω_i is the i^{th} natural frequency and ξ_i is the i^{th} modal damping factor. Now instead of solving N coupled equation of a N *DOF* system explained by Eq.(3.2), Eq.(3.6) enables to solve N decoupled single *DOF* which is much simpler.

3.4 Normal Mode Summation

In general, solving systems of large numbers of degrees of freedom is computationally expensive. It is possible, however, to reduce the computational time (or reduce the degrees of freedom of the system) by a procedure known as the mode summation method. Essentially, the displacement of the structure under forced excitation

is approximated by the sum of a limited number of normal modes of the system multiplied by generalized coordinates.

For example, consider a structure with 50 *DOF*. The solution of its undamped homogeneous equation will lead to 50 eigenvalues and 50 eigenvectors that describe the normal modes of the structure. If the excitation of the structure centers around the lower frequencies, the higher modes will not be excited and the forced response will be the superposition of only a few of the lower-frequency modes; perhaps $\phi_1(x), \phi_2(x)$, and $\phi_3(x)$ may be sufficient. Then the deflection under forced excitation can be written as

$$X_i = \phi_1(x_i)q_1(t) + \phi_2(x_i)q_2(t) + \phi_3(x_i)q_3(t) \tag{3.7}$$

or in matrix notation the displacement of all N degrees of freedom can be expressed in terms of the modal matrix $[\phi]$ composed of only three modes.

$$\begin{Bmatrix} X_1 \\ X_2 \\ . \\ . \\ X_N \end{Bmatrix} = \begin{bmatrix} \phi_1(X_1) & \phi_2(X_1) & \phi_3(X_1) \\ . & . & . \\ . & . & . \\ \phi_1(X_N) & \phi_2(X_N) & \phi_3(X_N) \end{bmatrix} \begin{Bmatrix} q_1 \\ q_2 \\ q_3 \end{Bmatrix} \tag{3.8}$$

The use of limited modal matrix then reduces the system to that equal to the number of modes used. For example, for the $50-DOF$ system, each of the matrices such as $[K]$ is a 50×50 matrix. Using three normal modes, $[\phi]$ is a 50×3 matrix and the product $[\phi]^T[K][\phi]$ is a $(3\times50)(50\times50)(50\times3)=(3\times3)$ matrix. Thus, instead of solving

the 50 coupled equations represented by Equations (3.2), it is required to only solve the three by three uncoupled equations represented by

$$[\phi]^T [M][\phi]\{\ddot{q}\} + [\phi]^T [C][\phi]\{\dot{q}\} + [\phi]^T [K][\phi]\{q\} = [\phi]^T \{F\} \tag{3.9}$$

It is noted that in this study the force excitation is not deterministic function of time. In fact, the input and output of the system are random processes which will be discussed in the next section.

3.5 Random Variable

There are a number of physical phenomena that result in nondeterministic data for which future instantaneous values cannot be predicted, such as noise of a jet engine pressure gusts, heights of waves and so on. Nondeterministic data of this type are referred to as random time functions. A sample of a typical random time function is shown in Figure3.1.

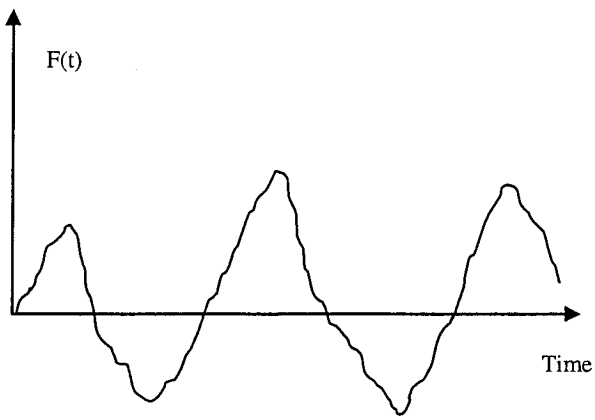

Fig. 3.2 A sample of random function

In this study, it is assumed that all random variables or functions are Guassian which can be characterized by their mean value and variance.

The covariance relationship of two variables is very useful in random analysis. Let assume n-dimensional vector X is related to n-dimensional vector Y, according to:

$$Y = PX \tag{3.10}$$

where P is a linear operator. Expanded form of Equation (3.10) can be written as:

$$\begin{bmatrix} Y_1 \\ Y_2 \\ . \\ Y_m \end{bmatrix} = \begin{bmatrix} P_{11} & P_{12} & . & . & . & P_{1n} \\ P_{21} & P_{22} & . & . & . & P_{2n} \\ . & & & & & \\ P_{m1} & P_{m2} & . & . & . & P_{mn} \end{bmatrix} \begin{bmatrix} X_1 \\ X_2 \\ . \\ X_n \end{bmatrix}$$

$$Y_i = \sum_{l=1}^{n} P_{il} X_l \qquad Y_j = \sum_{k=1}^{n} P_{jk} X_k \tag{3.11}$$

Thus $$E(Y_i Y_j) = \sum_{l=1}^{n} P_{il} \sum_{k=1}^{n} P_{jk} E(X_l X_k) \tag{3.12}$$

Now co-variance of Y and X may be related as:

$$[COVY] = [P]\ [COVX\ ]\ [P\ ]^T \tag{3.13}$$

where $m \times m$ matrix $[COVY]$ and $n \times n$ matrix $[COVX\ ]$ are covariance of X and Y, respectively.

Equation (3.13) will be used frequently in the following section to analyze stochastic performance at any structural point subjected to random excitation. The random process generates sequence of random variables in the time domain. The characteristics of a random process are discussed in next section.

3.6 Characteristics of Random Process

If random processes are stationary, they can be characterized effectively by the autocorrelation and cross-correlation in time domain. In any random process, a large number of data is necessary to establish reliability. For instance, to establish the statistics of the pressure fluctuation due to air turbulence in a certain air route, an airplane may collect hundreds of records of the type shown in Figure 3.3. Each record is called a

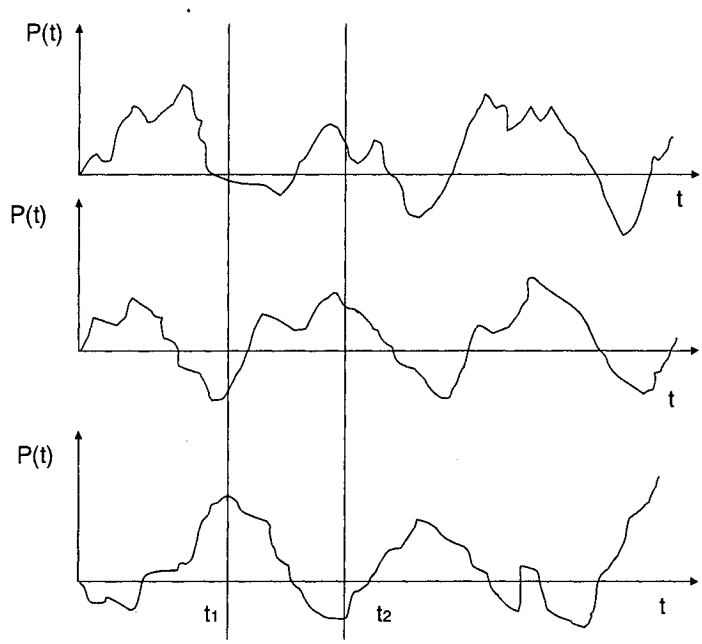

Fig.3.3 Three samples of the pressure fluctuation in a certain air routine

sample and the total collection of sample is called the ensemble. We can compute the ensemble average of the instantaneous pressure in each sample at time t_1. We can also multiply the instantaneous pressure in each sample at times t_1 and $t_1 + \Delta t$, and average

results for the ensembles. If such averages do not differ as we choose different values of the time, the random process described by this ensemble is said to be stationary.

The most important joint measure in a random process is the correlation of the process with itself in two different times, $x(t_1)$ with $x(t_2)$. Denoted $R_X(t_1,t_2)$, this measure of correlation is called the autocorrelation function expressed as:

$$R_X(t_1,t_2)= E[X(t_1)X(t_2)] \tag{3.14}$$

Similarly, cross-correlation is used to measure the correlation between two different random processes, say $X(t)$ and $Y(t)$, and it is defined as

$$R_{XY}(t_1,t_2)=E[X(t_1)Y(t_2)] \tag{3.15}$$

A strictly stationary process is difficult to demonstrate in practice. A more relaxed form of stationarity occurs when the mean and variance of the process are constants, and the autocorrelation function depends only on the difference between time t_1 and t_2, $R_X(t_1,t_2)= R_X(t_2-t_1)$. This process is called weakly stationary. Therefore, the stationary autocorrelation function is written in terms of the difference between t_1 and t_2, known as the lag, $\tau = t_2 - t_1$:

$$R_X(\tau)=R_X(t,\, t+\tau)= E[X(t)X(t+\tau)] \tag{3.16}$$

Since process X and Y are stationary, the cross-correlation can be written as

$$R_{XY}(\tau) = R_{XY}(t,\ t+\tau) = E[X(t)Y(t+\tau)] \tag{3.17}$$

The Fourier transform of the autocorrelation function is called the spectral density function (SDF) $S_X(\omega)$, which can be mathematically expressed as:

$$S_X(\omega) = \frac{1}{2\pi}\int_{-\infty}^{+\infty} R_X(\tau)e^{-i\omega\tau}d\tau \tag{3.18}$$

and its form transform pair is:

$$R_X(\tau) = \int_{-\infty}^{+\infty} S_X(\omega)e^{+i\omega\tau}d\omega \tag{3.19}$$

Spectral density function $S_X(\omega)$ can be used to characterize a stationary random process and to quantify random processes such as stochastic loading, acceleration, velocity, displacement and force. The spectral density function basically corresponds to the ensemble average of the squared moduli of the Fourier transform of $X(t)$. This suggests that we may estimate the spectral density function from a large number of sample realizations of $X(t)$. Spectral analyzers can be used to evaluate the spectral density function. For instance, the waveforms, represented by a current $i(t)$, or a voltage, $v(t)$ is iteratively filtered to a signal with only a single frequency. The filtered signal's mean-square value is then measured and plotted since i^2 and v^2 are proportional to power, this is called power at that frequency. The measured power is divided by the width of the

bands, analog the units i^2 or u^2 per unit frequency. Hence $S_x(\omega)$ is called power spectral density.

In similar, the cross-spectral density function is defined as the Fourier transform of the cross-correlation function. There are two cross-spectral density functions, $S_{XY}(\omega)$ and $S_{YX}(\omega)$, defined as follows:

$$S_{XY}(\omega) = \frac{1}{2\pi}\int_{-\infty}^{+\infty} R_{XY}(\tau)e^{-i\omega\tau}d\tau$$
$$S_{YX}(\omega) = \frac{1}{2\pi}\int_{-\infty}^{+\infty} R_{YX}(\tau)e^{+i\omega\tau}d\omega \tag{3.20}$$

It is noted that unlike the spectral density function, which is real valued, the cross-spectral density functions are complex. Similar to Equations (3.13), the relationship between spectral density function of two random processes $\{X\}$ and $\{Y\}$ related through $\{Y\} = [P]\{X\}$ may be described as:

$$[SPEC(Y)] = [P]^*[SPEC(X)]^*[P]^T \tag{3.21}$$

where $SPEC(Y)$ and $SPEC(X)$ are cross-spectral density functions of random process Y and X respectively.

3.7 Random Analysis of Multi-Degree-of-Freedom System

At this point, system's properties such as mass, stiffness and damping have been discussed completely in the previous sections, and excitations' characteristics including spectral density function, cross-spectral density functions, variance and (or) covariance

have also been stated clearly. The structure, its stochastic excitations and its performance response could be treated as an input-output system shown in Figure 3.4. The output is determined by input and system transformation function. In the analysis in this thesis, external noise is not considered.

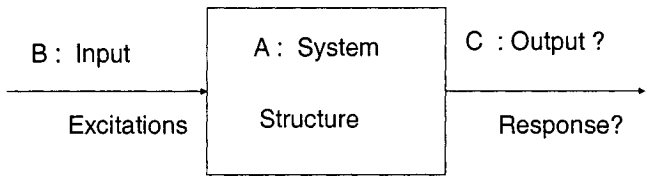

Fig. 3.4: Input, system and output

It was explained before that the equation of motion for a N $D.O.F$ system can be written in the form shown in Equation (3.2). To determine the cross-spectral density function of the response of the system, the approach is to employ the relationships between the spectral density function of a random process, $x(t)$, and the Fourier transform of $x(t)$. It can be shown that for a linear system, the response spectral density matrix $[S_X(\omega)]$ is related to the force spectral function $[S_F(\omega)]$ as:

$$[S_X(\omega)] = [H(\omega)][S_F(\omega)][H^*(\omega)] \tag{3.22}$$

The diagonal elements of $[S_X(\omega)]$ are the spectral density functions of each coordinate and the off-diagonal terms are the cross-spectral density functions and the matrix $[H(\omega)]$

and $[H^*(\omega)]$ are transform function and its transpose conjugate. Based on the spectral density functions, variance and covariance can subsequently be attained.

Rewriting Equation of motion in modal coordinates as explained in section 3.2, we have

$$\left[\bar{M}\right]\left\{\ddot{q}\right\}+\left[\bar{C}\right]\left\{\dot{q}\right\}+\left[\bar{K}\right]\{q\}=\{Q\} \tag{3.23}$$

Since $\{Q\}=[\phi]^T\{F\}$, the cross-spectral density function matrix of modal vector force $\{Q\}$ can be derived as

$$[S_Q(\omega)]=[\phi]^T[S_F(\omega)]\ [\phi] \tag{3.24}$$

thus, the cross-spectral density function matrix of modal response coordinate $\{q\}$ may be expressed as:

$$[S_q(\omega)]\ =[H(\omega)]\ [\phi]^T\ [S_F(\omega)]\ [\phi]\ [H^*(\omega)] \tag{3.25}$$

Consider that $\{X\}=[\phi]\{q\}$, thus, the spectral density function matrix of $\{X\}$ is

$$S_X(\omega)=[\phi]\ [S_q(\omega)]\ [\phi]^T\ =[\phi]\ [H(\omega)][\phi]^T\ [S_F(\omega)]\ [\phi]\ [H^*(\omega)][\phi]^T \tag{3.26}$$

Equation (3.26) is fundamental relation for multi-degree-of-freedom system under random loading. Using normal mode method, $[H(\omega)]$ can easily be obtained and is diagonal. Every mode transform function such as $H_j(\omega)$ has real and imaginary part.

It is noted that calculation of the response spectral density function in Equation (3.26) is computationally expensive. On the other hand, it is unnecessary to calculate the

spectral density function of the whole system. Assuming that the system has N degree-of-freedom, it would be very costly to obtain the spectral density function which is $N \times N$ matrix. Thus it is more efficient to employ normal mode summation technique considering only the first few modes.

For convenience, let us rewrite equation (3.8) as:

$$\begin{Bmatrix} X_1 \\ X_2 \\ . \\ . \\ X_N \end{Bmatrix} = \begin{bmatrix} \phi_1(X_1) & \phi_2(X_1) & \phi_3(X_1) \\ . & . & . \\ . & . & . \\ \phi_1(X_N) & \phi_2(X_N) & \phi_3(X_N) \end{bmatrix} \begin{Bmatrix} q_1 \\ q_2 \\ q_3 \end{Bmatrix}$$

where, the modal matrix $[\phi]$ may be written as:

$$[\phi] = \begin{bmatrix} \phi_{11} & \phi_{12} & \phi_{13} \\ \phi_{21} & \phi_{22} & \phi_{23} \\ \phi_{31} & \phi_{32} & \phi_{33} \\ . & . & . \\ \phi_{N1} & \phi_{N2} & \phi_{NN} \end{bmatrix}_{N\times 3} \qquad [\phi]^T = \begin{bmatrix} \phi_{11} & \phi_{21} & \phi_{31} \cdot \cdot \cdot & \phi_{N1} \\ \phi_{12} & \phi_{22} & \phi_{32} \cdot \cdot \cdot & \phi_{N2} \\ \phi_{13} & \phi_{23} & \phi_{33} \cdot \cdot \cdot & \phi_{N3} \end{bmatrix}_{3\times N}, \qquad (3.27)$$

Now Equation (3.26) can be expressed as:

$$[S_q(\omega)] = \begin{bmatrix} H_1(\omega) & 0 & 0 \\ 0 & H_2(\omega) & 0 \\ 0 & 0 & H_3(\omega) \end{bmatrix} \begin{bmatrix} S_{Q_{11}} & S_{Q_{12}} & S_{Q_{13}} \\ S_{Q_{21}} & S_{Q_{22}} & S_{Q_{23}} \\ S_{Q_{31}} & S_{Q_{32}} & S_{Q_{33}} \end{bmatrix} \begin{bmatrix} H_1^*(\omega) & 0 & 0 \\ 0 & H_2^*(\omega) & 0 \\ 0 & 0 & H_3^*(\omega) \end{bmatrix}$$

$$= \begin{bmatrix} S_{q_{11}} & S_{q_{12}} & S_{q_{13}} \\ S_{q_{21}} & S_{q_{21}} & S_{q_{21}} \\ S_{q_{31}} & S_{q_{32}} & S_{q_{33}} \end{bmatrix} \qquad (3.28)$$

$$S_{q_{kl}} = S_{Q_{kl}} H_k(\omega) H_l^*(\omega) \qquad \begin{matrix} k = 1,\ 2,\ 3 \\ l = 1,\ 2,\ 3 \end{matrix} \tag{3.29}$$

It is noted that using Equation (3.29), components of spectral density function can be easily calculated. Also using Eq.(3.24), the spectral density matrix $[S_Q(\omega)]$ may be written as:

$$[S_Q(\omega)] = [\phi]^T S_F(\omega)[\phi]$$

$$= \begin{bmatrix} \phi_{11} & \phi_{21} & \phi_{31} \cdots & \phi_{N1} \\ \phi_{12} & \phi_{22} & \phi_{32} \cdots & \phi_{N2} \\ \phi_{13} & \phi_{23} & \phi_{33} \cdots & \phi_{N3} \end{bmatrix}_{3\times N} \begin{bmatrix} S_{F_{11}} & S_{F_{12}} & S_{F_{13}} \cdots & S_{F_{1N}} \\ S_{F_{21}} & S_{F_{22}} & S_{F_{23}} \cdots & S_{F_{2N}} \\ \cdot & & & \\ \cdot & & & \\ S_{F_{N1}} & S_{F_{N2}} & S_{F_{N3}} \cdots & S_{F_{NN}} \end{bmatrix}_{N\times N} \begin{bmatrix} \phi_{11} & \phi_{12} & \phi_{13} \\ \phi_{21} & \phi_{22} & \phi_{23} \\ \phi_{31} & \phi_{32} & \phi_{33} \\ \cdot & & \\ \cdot & & \\ \phi_{N1} & \phi_{N2} & \phi_{N3} \end{bmatrix}_{N\times 3}$$

$$= \begin{bmatrix} \sum_{i}^{N} \phi_{i1} S_{F_{i1}} & \sum_{i=1}^{N} \phi_{i1} S_{F_{i2}} \cdots & \sum_{i=1}^{N} \phi_{i1} S_{F_{iN}} \\ \sum_{i=1}^{N} \phi_{i2} S_{F_{i1}} & \cdot & \cdot \\ \cdot & \cdot & \sum_{i=1}^{N} \phi_{iN} S_{F_{iN}} \end{bmatrix}_{3\times N} \begin{bmatrix} \phi_{11} & \phi_{12} & \phi_{13} \\ \phi_{21} & \phi_{22} & \phi_{23} \\ \phi_{31} & \phi_{32} & \phi_{33} \\ \cdot & & \\ \cdot & & \\ \phi_{N1} & \phi_{N2} & \phi_{N3} \end{bmatrix}_{N\times 3}$$

$$= \begin{bmatrix} S_{Q_{11}} & S_{Q_{12}} & S_{Q_{13}} \\ S_{Q_{21}} & S_{Q_{22}} & S_{Q_{23}} \\ S_{Q_{31}} & S_{Q_{32}} & S_{Q_{33}} \end{bmatrix} \tag{3.30}$$

thus, the term of S_{ab} in the matrix $[S_Q(\omega)]$ can be described by:

$$S_{Q_{ab}} = \sum_{i=1}^{N} \varphi_{ia} S_{F_{i1}} \varphi_{1b} + \sum_{i=1}^{N} \varphi_{ia} S_{F_{i2}} \varphi_{2b} + \cdots + \sum_{i=1}^{N} \varphi_{ia} S_{F_{iN}} \varphi_{Nb} \tag{3.31}$$

$$= \sum_{j=1}^{N}\sum_{i=1}^{N} \phi_{ia} S_{F_{ij}} \phi_{jb} = \sum_{i=1}^{N}\sum_{j=1}^{N} \phi_{ia} S_{F_{ij}} \phi_{jb}$$

After evaluating the modal spectral density function, the spectral density function in original coordinate can be obtained as:

$$[S_X(\omega)] = [\phi][S_q(\omega)][\phi]^T$$

$$= \begin{bmatrix} \phi_{11} & \phi_{12} & \phi_{13} \\ \phi_{21} & \phi_{22} & \phi_{23} \\ \phi_{31} & \phi_{32} & \phi_{33} \\ \cdot & & \\ \cdot & & \\ \phi_{N1} & \phi_{N2} & \phi_{N3} \end{bmatrix}_{N\times 3} \begin{bmatrix} S_{q11} & S_{q12} & S_{q13} \\ S_{q21} & S_{q22} & S_{q23} \\ S_{q31} & S_{q32} & S_{q33} \end{bmatrix}_{3\times 3} \begin{bmatrix} \phi_{11} & \phi_{21} & \phi_{31} & \cdot & \cdot & \phi_{N1} \\ \phi_{12} & \phi_{22} & \phi_{32} & \cdot & \cdot & \phi_{N2} \\ \phi_{13} & \phi_{23} & \phi_{33} & \cdot & \cdot & \phi_{N3} \end{bmatrix}_{3\times N}$$

$$= \begin{bmatrix} \sum_{i=1}^{3} \phi_{1i} S_{q_{i1}} & \sum_{i=1}^{3} \phi_{1i} S_{q_{i2}} & \sum_{i=1}^{3} \phi_{1i} S_{q_{i3}} \\ \cdot & \cdot & \cdot \\ \cdot & \cdot & \cdot \\ \cdot & \cdot & \cdot \\ \sum_{i=1}^{3} \phi_{Ni} S_{q_{i1}} & \sum_{i=1}^{3} \phi_{Ni} S_{q_{i2}} & \sum_{i=1}^{3} \phi_{Ni} S_{q_{i3}} \end{bmatrix}_{N\times 3} \begin{bmatrix} \phi_{11} & \phi_{21} & \phi_{31} & \cdot & \cdot & \phi_{N1} \\ \phi_{12} & \phi_{22} & \phi_{32} & \cdot & \cdot & \phi_{N2} \\ \phi_{13} & \phi_{23} & \phi_{33} & \cdot & \cdot & \phi_{N3} \end{bmatrix}_{3\times N} \tag{3.32}$$

$$= \begin{bmatrix} S_{X_{11}} & S_{X_{12}} & \cdot & \cdot & \cdot & S_{X_{1N}} \\ \cdot & & & & & \\ \cdot & & & & & \\ \cdot & & & & & \\ S_{X_{N1}} & S_{X_{N2}} & \cdot & \cdot & \cdot & S_{X_{NN}} \end{bmatrix}_{N\times N}$$

Thus, the term $S_{X_{cd}}$ is the element of response spectral density matrix. $[S_X(\omega)]$ and can be written as:

$$S_{X_{cd}} = \sum_{i=1}^{3} \phi_{ci} S_{q_{i1}} \phi_{d1} + \sum_{i=1}^{3} \phi_{ci} S_{q_{i2}} \phi_{d2} + \sum_{i=1}^{3} \phi_{ci} S_{q_{i3}} \phi_{d3}$$
$$= \sum_{j=1}^{3}\sum_{i=1}^{3} \phi_{ci} S_{q_{ij}} \phi_{dj} = \sum_{i=1}^{3}\sum_{j=1}^{3} \phi_{ci} S_{q_{ij}} \phi_{dj} \tag{3.33}$$

Let us substitute the spectral density function of modal force $[S_Q]$, from Equation (3.30) into Equation (3.29)

$$S_{q_{ab}} = \sum_{i=1}^{N}\sum_{j=1}^{N} \phi_{ia} S_{F_{ij}} \phi_{jb} H_a(\omega) H_b^*(\omega) \tag{3.34}$$

Now substitution of Equation (3.34) into Equation (3.32), yields:

$$S_{X_{cd}} = \sum_{i=1}^{3}\sum_{j=1}^{3} \phi_{ci}\phi_{dj} \left(\sum_{s=1}^{N}\sum_{k=1}^{N} \phi_{si}\phi_{kj} S_{F_{sk}} H_i(\omega) H_j^*(\omega) \right) \tag{3.35}$$

or

$$S_{Xcd} = \sum_{i=1}^{3}\sum_{j=1}^{3} \phi_{ci}\phi_{dj} \left(\sum_{s=1}^{N}\sum_{k=1}^{N} \phi_{si}\phi_{kj} S_{F_{sk}} H_j(\omega) H_i^*(\omega) \right) \tag{3.36}$$

It is noted that only real part of cross-spectral is meaningful, and the integration of imaginary part is zero. As a result, formulas (3.35) and (3.36) are equivalent, and both can be used to calculate variance and covariance.

Equations (3.35) and (3.36) are exact solutions to obtain covariance of multi D.O.F system in random problems. It does not need any additional assumptions. The great value of this method is that the covariance matrix can be precisely obtained which can lead to any performance randomness in continuous structure.

3.8 Finite Element Model of Continuous Structure Subjected to Random Excitations

Because random environments discussed include base excitation to continuous structure, it is very necessary to set up its finite element model. Using finite element method, the characteristics of the structure such as inertia and stiffness can be obtained. In other words, the matrices $[M]$ and $[K]$ can be established by using the finite element method. For the sake of simplicity, let us assume the system has 4 DOF, then kinetic energy T of the system can be written as;

Kinetic energy T of the whole system is

$$T = \frac{1}{2}\begin{bmatrix} \dot{v}_1 & \dot{v}_2 & \dot{v}_3 & \dot{v}_4 \end{bmatrix}\begin{bmatrix} m_{11} & m_{12} & m_{13} & m_{14} \\ m_{21} & m_{22} & m_{23} & m_{24} \\ m_{31} & m_{32} & m_{33} & m_{34} \\ m_{41} & m_{42} & m_{43} & m_{44} \end{bmatrix}\begin{bmatrix} \dot{v}_1 \\ \dot{v}_2 \\ \dot{v}_3 \\ \dot{v}_4 \end{bmatrix} \tag{3.37}$$

where v_1, v_2, v_3 and v_4 are the displacements at degrees of freedom 1,2,3, and 4 respectively and $\dot{v}_1, \dot{v}_2, \dot{v}_3$ and $\dot{v}_4$ are velocities. Assume that degree of freedom 1 is subjected to a random acceleration excitation with power spectral density function. Objective is to find response of the other degrees of freedom. Knowing this, let us rewrite the kinetic energy in the following form,

$$T = \frac{1}{2}\left(\dot{v}_1 m_{11} \dot{v}_1 \right) + \frac{1}{2}\left[(m_{12}+m_{21})\dot{v}_1 + (m_{13}+m_{31})\dot{v}_1 + (m_{14}+m_{41})\dot{v}_1 \right] \begin{bmatrix} \dot{v}_2 \\ \dot{v}_3 \\ \dot{v}_4 \end{bmatrix}$$

$$+ \frac{1}{2} \begin{bmatrix} \dot{v}_2 \\ \dot{v}_3 \\ \dot{v}_4 \end{bmatrix} \begin{bmatrix} m_{22} & m_{23} & m_{24} \\ m_{32} & m_{33} & m_{34} \\ m_{42} & m_{43} & m_{44} \end{bmatrix} \begin{bmatrix} \dot{v}_2 \\ \dot{v}_3 \\ \dot{v}_4 \end{bmatrix} \tag{3.38}$$

The expression in Eq.(3.38) can be treated as the combination of two systems. System 1 has one degree-of-freedom which is known. System 2 has three degrees-of-freedom which needs to be solved. The total kinetic energy of system 2 is given by

$$T_2 = \frac{1}{2}\left[(m_{12}+m_{21})\dot{v}_1 + (m_{13}+m_{31})\dot{v}_1 + (m_{14}+m_{41})\dot{v}_1 \right] \begin{bmatrix} \dot{v}_2 \\ \dot{v}_3 \\ \dot{v}_4 \end{bmatrix}$$

$$+ \frac{1}{2} \begin{bmatrix} \dot{v}_2 \\ \dot{v}_3 \\ \dot{v}_4 \end{bmatrix}^T \begin{bmatrix} m_{22} & m_{23} & m_{24} \\ m_{32} & m_{33} & m_{34} \\ m_{42} & m_{43} & m_{44} \end{bmatrix} \begin{bmatrix} \dot{v}_2 \\ \dot{v}_3 \\ \dot{v}_4 \end{bmatrix} \tag{3.39}$$

The potential energy of system 2 can also be expressed as:

$$U_2 = \frac{1}{2}\left[(k_{12}+k_{21})v_1 + (k_{13}+k_{31})v_1 + (k_{14}+k_{41})v_1 \right] \begin{bmatrix} v_2 \\ v_3 \\ v_4 \end{bmatrix}$$

$$+\frac{1}{2}\begin{bmatrix} v_2 \\ v_3 \\ v_4 \end{bmatrix}^T \begin{bmatrix} k_{22} & k_{23} & k_{24} \\ k_{32} & k_{33} & k_{34} \\ k_{42} & k_{43} & k_{44} \end{bmatrix} \begin{bmatrix} v_2 \\ v_3 \\ v_4 \end{bmatrix} \tag{3.40}$$

According to Hamilton's principle and Lagrange's equations, the undamped motion equation of freedom v_2, v_3 and v_4 with respect to v_1 can be described by:

$$[M]_{3\times3}\left\{\ddot{v}\right\}_{3\times1} + [K]_{3\times3}\{v\}_{3\times1} = -\begin{Bmatrix} \frac{1}{2}(m_{12}+m_{21})\ddot{v}_1 + \frac{1}{2}(k_{12}+k_{21})v_1 \\ \frac{1}{2}(m_{13}+m_{31})\ddot{v}_1 + \frac{1}{2}(k_{13}+k_{31})v_1 \\ \frac{1}{2}(m_{14}+m_{41})\ddot{v}_1 + \frac{1}{2}(k_{14}+k_{41})v_1 \end{Bmatrix} \tag{3.41}$$

Eq.(3.41) can be interpreted as the finite element model of continuous structure which is subjected to base excitation. It is noted that this formula can apply to any structure under any boundary conditions. Using this model, dynamic response of continuous structure excited by base motion can be obtained.

If the base excitations are stochastic, randomness characterization of the general forces should be obtained in order to predict structure behavior. The general force vector is given in the right side of equation (3.41).Since spectral density function of random process $\ddot{v}_1$ is given by $S_{\ddot{v}_1}(\omega)$, the spectral density function of $\dot{v}_1$ is $\frac{1}{\omega^2} S_{\ddot{v}_1}(\omega)$ and the

spectral density function of $\ddot{v}_1$ is given by $\frac{1}{\omega^4} S_{\ddot{v}_1}(\omega)$. After that, the spectral density function matrix of general force vector can be obtained.

Finally, the randomness of the displacements can then be attained. The above basic derivation can be applied to other complex structure.

3.9 Model Verification

In section 3.7, modeling of performance response for multi D.O.F system has been developed. This model will be verified with already published results. As not many results were available for comparison, the results are compared with the results of [8]. The following is the verification of this modeling by a two-degree-of-freedom system. The system and the excitation are shown in Figure 3.5.

$$w_0 = 0.070\ m^2/\sec^4/HZ, m_1 = 35kg, m_2 = 17.5kg,\ k_1 = 8750N/m,\quad k_2 = 3500N/m$$

The assumed damping factors for each mode are

$$\xi_1 = 0.037$$
$$\xi_2 = 0.053$$

Set x_1 and x_2 as absolute displacement of mass m_1 *and* m_2 respectively.

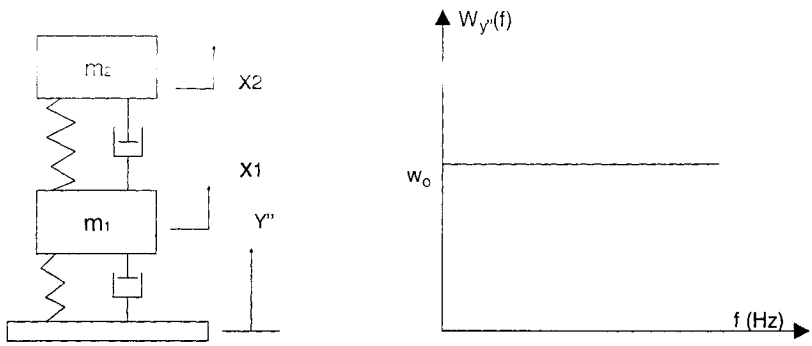

Fig.3.5 Two-degree-of-freedom system and spectral density of base acceleration

The undamped governing differential equations of motion can be written as:

$$[M]\{X\}+[K]\{Z\}=0 \tag{3.42}$$

where $\{Z\}=\{X\}-Y$ is the relative displacement and Y is the base displacement. Rearranging the Eq. (3.42), we may have:

$$[M]\left\{\ddot{Z}\right\}+[K]\{Z\}=\{F\} \tag{3.43}$$

where $\{F\}=\begin{Bmatrix}-m_1\ddot{Y}\\ -m_2\ddot{Y}\end{Bmatrix}$ and the spectral density function $[S_F(\omega)]$ of nodal force $\{F\}$ can be described by:

$$[S_F(\omega)]=\begin{bmatrix}m_1^2 w_o & m_1 m_2 w_o\\ m_2 m_1 w_o & m_2^2 w_o\end{bmatrix} \tag{3.44}$$

where w_0 is the spectral density function of base acceleration excitation. Using the performance prediction modeling expressed in Equation (3.36), the covariance of relative displacement can be obtained as:

$$E[X_c, X_d] = \sum_{i=m}^{n}\sum_{j=m}^{n}\phi_{ci}\phi_{dj}\left(\sum_{s=Ai}^{Ae}\sum_{Ai=1}^{Ae}\phi_{si}\phi_{kj}\int_{-\infty}^{+\infty}S_{Fsk}H_j(\omega)H_i^*(\omega)d\omega\right) \tag{3.45}$$

$$[COVZ] = \begin{bmatrix} 7.1759\times10^{-5} & 1.5970\times10^{-4} \\ 1.5970\times10^{-4} & 3.8256\times10^{-4} \end{bmatrix} \tag{3.46}$$

where, $[COVZ]$ is covariance of relative displacements $\{z\}$. The standard deviation of relative displacements Z_1 and Z_2 are found to be:

$$\sigma_{z1} = 8.46\ mm \quad , \quad \sigma_{z2} = 19.56\ mm \tag{3.47}$$

Now from the normal mode transformation, we can have:

$$\begin{aligned} Z_1 &= \phi_{11}q_1 + \phi_{12}q_2 \\ Z_2 &= \phi_{21}q_1 + \phi_{22}q_2 \end{aligned} \tag{3.48}$$

where $[\phi] = \begin{bmatrix} 1 & 1 \\ 2.35 & -0.85 \end{bmatrix}$ is the modal matrix and the transformation to modal coordinates can be described as:

$$\begin{bmatrix} z_1 \\ z_2 \end{bmatrix} = \begin{bmatrix} 1 & 1 \\ 2.35 & -0.85 \end{bmatrix}\begin{bmatrix} q_1 \\ q_2 \end{bmatrix} \tag{3.49}$$

The nodal force can be obtained from:

$$\{Q\} = [\phi]^T\{F\} = \begin{bmatrix} -76.1\ddot{Y} \\ -20.1\ddot{Y} \end{bmatrix} \tag{3.50}$$

Since Y is white noise, we can use the white-noise formulas

$$\sigma_{Zi}^2 = \frac{W_0}{1984\xi f_i} \tag{3.51}$$

where W_0 is spectral density function of i^{th} nodal force, ξ_i is i^{th} damping ratio, and

f_i is i^{th} frequency. Therefore, the variances of modal coordinates q_1, q_2 are

$$\sigma_1^2 = \frac{(0.578)^2(0.0742)}{1984(0.034)(1.71)^3} = 7.35\times10^{-5}$$
$$\sigma_2^2 = \frac{(0.422)^2(0.0742)}{1984(0.066)(3.32)^3} = 2.76\times10^{-6} \tag{3.52}$$

The problem here is that the correlation coefficient about random processes q_1 and q_2 is not clear. It is assumed that these two processes are independent (this assumption will result in insignificant errors). Therefore, the variances based on this method are approximate solutions.

$$\begin{aligned}\sigma_{z1}^2 &= \phi_{11}^2\sigma_1^2 + \phi_{12}^2\sigma_2^2 = (1)(7.35\times10^{-5}) + (1)(2.76\times10^{-6}) \\ &= 73.5\times10^{-6} + 2.76\times10^{-6} = 76.26\times10^{-6} \\ \sigma_{z2}^2 &= \phi_{21}^2\sigma_1^2 + \phi_{22}^2\sigma_2^2 = (2.35^2)(7.35\times10^{-5}) + (0.85^2)(2.76\times10^{-6}) \\ &= (405.9 + 1.994)\times10^{-6}\end{aligned} \tag{3.53}$$

Thus the values of the standard deviations of the relative displacement using normal method approximations are found to be:

$$\sigma_{z1} = 8.73\,mm \quad , \quad \sigma_{z2} = 20.19\,mm \tag{3.54}$$

Comparing the results in Eqs. (3.47) and (3.54), it can be realized that there is only 4% difference which is generally considered acceptable. Therefore, it can be concluded that the dynamic modeling formulated in Eq. (3.36) can be applied accurately to any multi-degree-of-freedom systems.

CHAPTER 4

MICROMECHANICAL STRUCTURES

In the previous chapter, the dynamic performance of mechanical structures with multi-degree-of-freedom has been modeled and studied. As this thesis aims at predicting the performances of micro-structures under random environments, this chapter will apply the dynamic prediction models to MEMS structures.

4.1 Random Environments of MEMS Structures

4.1.1 Random base excitation

As discussed earlier, MEMS have wide applications in automobile and aerospace industries and are subjected to random environments. The operating environments of MEMS structure used for the above applications are considered as typical examples for the present study, and will be discussed in this Chapter. In this section, two types of random environments will be discussed. They are stochastic base excitation, and stochastic loading which is due to random measurements. Figure 4.1 schematically shows a MEMS structure subjected to both random loading and random base excitation. In this figure, because the measurements such as pressure, acceleration have random nature, the MEMS structures used to measure this parameters are subjected to random loading,

consequently. Meanwhile, MEMS are attached to vehicles and (or) flight articles, so if the bodies are vibrating randomly, the MEMS structures will undergo random base excitation.

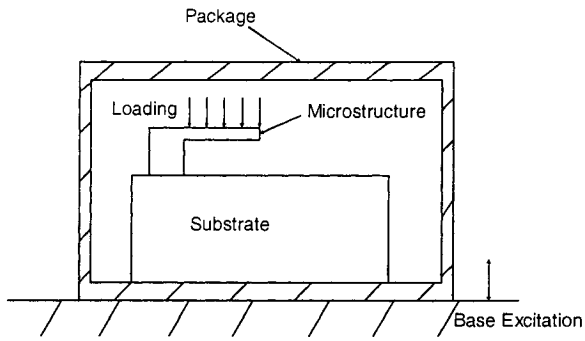

Fig. 4.1 Scheme showing a micro-structure subjected to random loading and random base excitation

For example, automobile vehicles are subjected to random excitation due to pavement roughness as shown in Figure 1.8. Since the surface roughness profile is regarded as a random function, it can be characterized by a spatial power spectral density function $W_S(f_S)$, which is a function of spatial frequency f_S (cycles/m). It is known that the relationship between the spatial spectral density function and the spatial frequency for the ground profiles can be approximated by:

$$W_S(f_S) = C_{SP} f_s^{-N} \tag{4.1}$$

where C_{SP} and N are constants that depend on the road conditions. Values of C_{SP} and N for

various surfaces are given in Table 4.1.

Table 4.1 Values of C_{sp} and N

No.	Description	N	C_{sp}
1	Smooth runway	3.8	4.3×10^{-11}
2	Rough runway	2.1	8.1×10^{-6}
3	Smooth highway	2.1	4.8×10^{-7}
4	Highway with gravel	2.1	4.4×10^{-6}

For vehicle vibration analysis, it is more convenient to express the power spectral density of surface profiles in terms of frequency f in Hz rather than in terms of the spatial frequency in cycle/m, since vehicle vibration is a function of time. Transformations of the spatial frequency f_s to the frequency f and spatial power spectral density $W_s(f_s)$ to power spectral density $W_\eta(f)$ can be established through the speed of the vehicle V in m/s. The transformations can be given by (4.2) and (4.3) respectively.

$$f = f_s V \tag{4.2}$$

and

$$W_s(f_s) = V W_\eta(f) \tag{4.3}$$

where, f is frequency, f_s is spatial frequency, W_η is power spectral density function of road profile, W_s is spatial power spectral density function.

Thus, we get

$$W_\eta(f) = \frac{W_s(f_s)}{V} = \frac{C_{sp} f_s^{-N}}{V} = \frac{C_{SP}\left(\frac{f_s}{V}\right)^{-N}}{V} \tag{4.4}$$

Based on equation (4.4), power spectral density function of pavement roughness can be obtained. For example, Figure 4.2 gives the typical randomness characteristic of smooth highway surface when a vehicle velocity is $80 Km/h$.

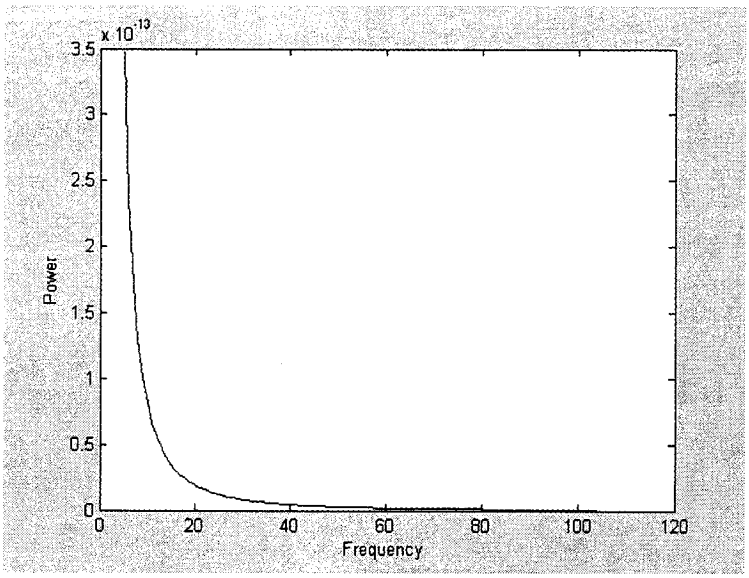

Fig. 4.2: Power spectral density of rough runway when velocity is $80\, km/h$

The whole vehicle structure will vibrate randomly due to the road roughness shown in Figure 4.2. Consequently, all MEMS structures attached in the vehicle will undergo random base excitation. In order to study this base excitation, a walking-beam model is given in Figure 4.3.

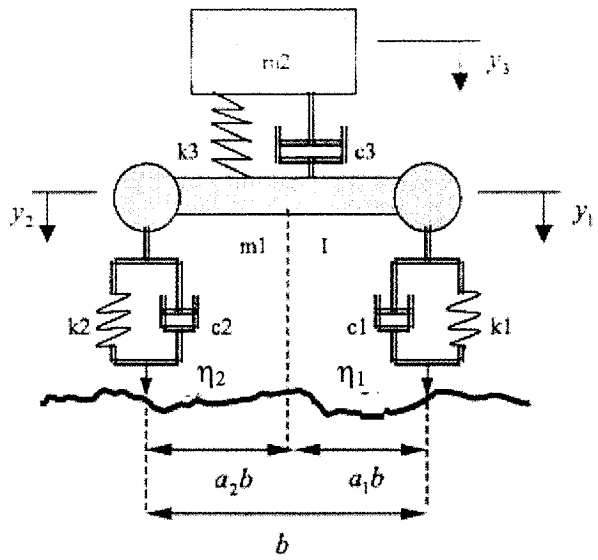

Fig. 4.3 Mathematical vehicle model in stochastic roughness road [31]

Table 4.2 Descriptions of parameters used in the vehicle suspension model

Parameters	Descriptions
m_1	Unsprung mass
m_2	Sprung mass
I	Moment inertia of unsprung mass
k_1	Right-side tire spring stiffness
k_2	Left-side tire spring stiffness
k_3	Suspension spring stiffness
c_1	Right-side tire damping
c_2	Left-side tire damping
c_3	Suspension damping
b	Effective width of the vehicle
y_1	Absolute vertical displacement of right-side of unsprung mass
y_2	Absolute vertical displacement of left-side of unsprung mass
y_3	Absolute vertical displacement sprung mass
η_1	Absolute height of pavement profile corresponding to right-side tire
η_2	Absolute height of pavement profile corresponding to right-side tire

The equation of motion of the system shown in Figure 4.3 can be given by (4.5).

$$M\left\{\ddot{Z}\right\}+C\left\{\dot{Z}\right\}+K\{Z\}=\{F\} \tag{4.5}$$

where $\{\ddot{Z}\} = \{\ddot{z}_1, \ddot{z}_2, \ddot{z}_3\}^T$, $\{\dot{Z}\} = \{\dot{z}_1, \dot{z}_2, \dot{z}_3\}^T$, $\{Z\} = \{z_1, z_2, z_3\}^T$

and $z_1 = y_1 - \eta_1$, $z_2 = y_2 - \eta_2$, and $z_3 = y_3$. As the road excitation to the vehicle system, here η_1 and η_2 are the respective pavement profiles corresponding to right and left tires. Furthermore, mass matrix $[M]$, damping matrix $[C]$, stiffness matrix $[K]$ and force vector F are, respectively given by:

$$M = \begin{bmatrix} 0 & 0 & m_2 \\ m_1 a_1 & m_2 a_2 & 0 \\ -I/b & I/b & 0 \end{bmatrix}, \quad C = \begin{bmatrix} -c_3 a_2 & -c_3 a_1 & c_3 \\ c_1 + c_3 a_2 & c_2 + c_3 a_1 & -c_3 \\ c_1 a_2 b & -c_2 a_1 b & 0 \end{bmatrix},$$

$$K = \begin{bmatrix} -k_3 a_2 & -k_3 a_1 & k_3 \\ k_1 + k_3 a_2 & k_2 + k_3 a_1 & -k_3 \\ k_1 a_2 b & -k_2 a_1 b & 0 \end{bmatrix} \tag{4.6}$$

$$F = \begin{bmatrix} 0 & c_3 a_2 & k_3 a_2 & 0 & c_3 a_1 & k_3 a_1 \\ -m_1 a_2 & -c_3 a_2 & -k_3 a_2 & -m_1 a_1 & -c_3 a_1 & -k_3 a_1 \\ I/b & 0 & 0 & -I/b & 0 & 0 \end{bmatrix} \begin{Bmatrix} \ddot{\eta}_1 \\ \dot{\eta}_1 \\ \eta_1 \\ \ddot{\eta}_2 \\ \dot{\eta}_2 \\ \eta_2 \end{Bmatrix}$$

The commonly used description of a pavement roughness is to define a road profile in longitudinal direction as a one-dimensional random field as shown in Eq.(4.4) and Figure (4.2). To simply the above study, a widely accepted assumption is given that the pavement surface can be treated as isotropic homogenous random field [32]. According

to the assumption of isotropy, the spectral density function roughness of each individual profile under two sides of axle remains the same as the one-dimensional spectral density function roughness.

Thus, the cross spectral density function of generalized force vector expressed in Eq.(4.6) can be obtained. With the response modeling proposed in Chapter 3, cross spectral density function matrix $S_Z(\omega)$ of response $\{Z\} = \{z1, z2, z3\}^T$ can be obtained. MEMS structures are subjected to different random vibrations according to the location they are attached. Take the right-side tire pressure sensor for instance, the MEMS structures undergo random base excitation, and it's randomness is characterized by spectral density function of right-side tire vertical displacement $S_{Z_1}(\omega)$ which is the first diagonal term of $S_Z(\omega)$. Furthermore, based on $S_{Z_1}(\omega)$, the fluctuation of tire pressure can also be developed, the details will be presented in the next section.

As discussed above, MEMS structures in automobile applications might be subjected to random base excitation due to random road roughness. In the applications to space industry, MEMS structures are also commonly under the random vibration environment. This random vibration occurs over a broad frequency range, from about 10 Hz to 2000 Hz which is directly transmitted into the flight article through its mounts from the launch vehicle sources such as engine firing, turbo-pumps, etc. Figure 4.4 is the

typical Power Spectral Density of such random vibration transmitted to flight article. Thus, MEMS structures attached to flight articles are subjected to serious random base excitation, especially, during the launching period.

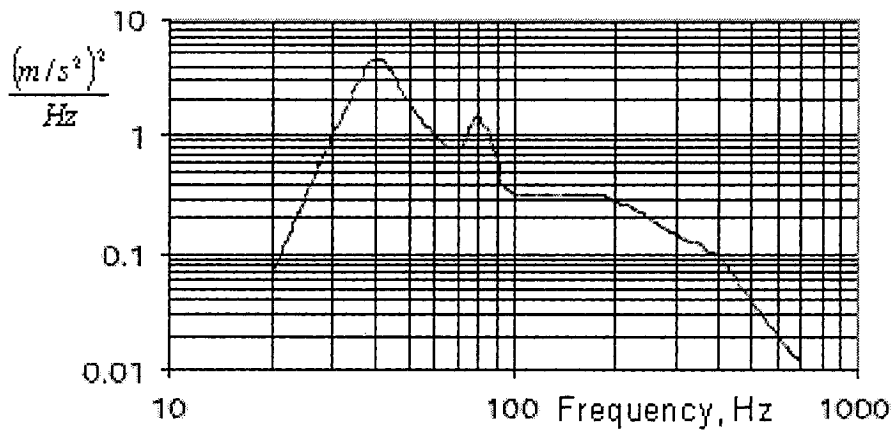

Fig. 4.4 Random vibration levels transmitted to flight article through mounts, the power unit is $(m/s^2)^2/Hz$ [1]

According to different operating environment, the requirement of the ability of MEMS structure to endure random vibration is therefore different. Figure 4.5 is the sample of the SDF of minimum vibration level proposed by NASA[1] that can be used for MEMS defect detection.

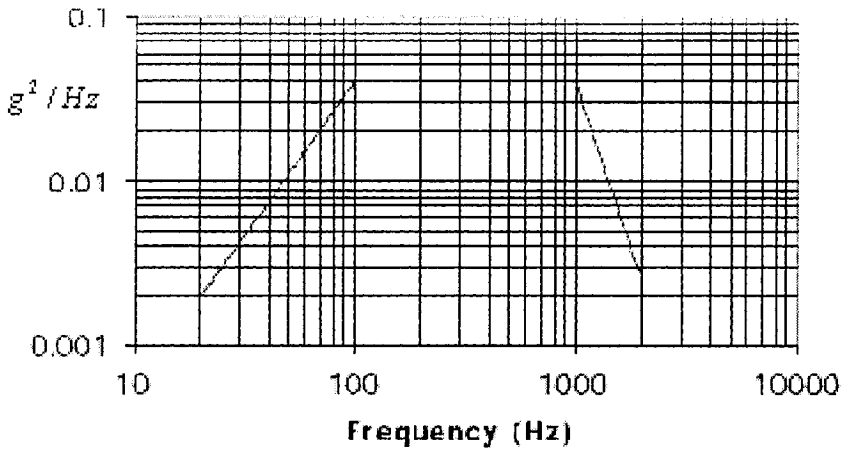

Fig. 4.5 Minimum vibration levels for MEMS defect detection, vibration unit is g^2/Hz [1]

4.1.2 Random loading

MEMS structures are subjected to random loading directly due to the random nature of the measurements. If the pressure is random, the MEMS structures in Figures 4.6 and 4.7 will be subjected to random loading. Similarly, stochastic acceleration and angular velocity rate will result in that the MEMS structures shown in Figures 4.8 and 4.9 undergo random loadings. In this section, as an example of random loading, the relationship between the road roughness and tire pressure fluctuation will be explored.

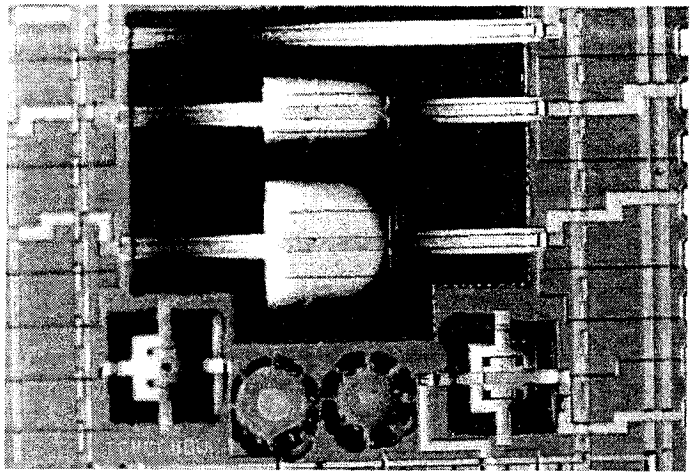

Fig. 4.6 Beam-plate inertial capacitive MEMS sensors fabricated in Concordia

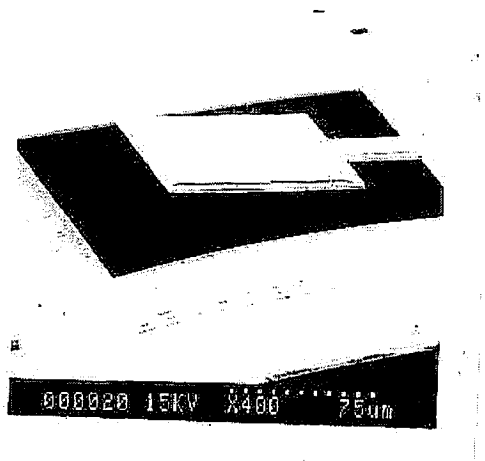

Fig. 4.7 Scanning electron micrograph of a beam- plate type pressure sensor fabricated in Concordia

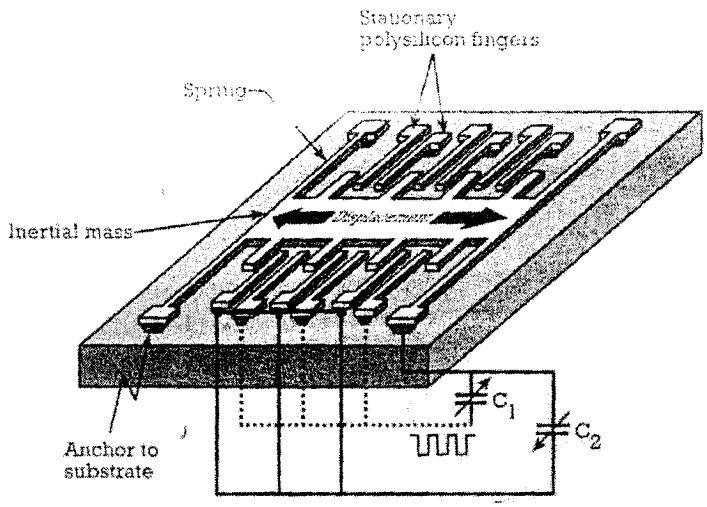

Fig. 4.8 Beam-plate type surface-micromachined accelerometer [34]

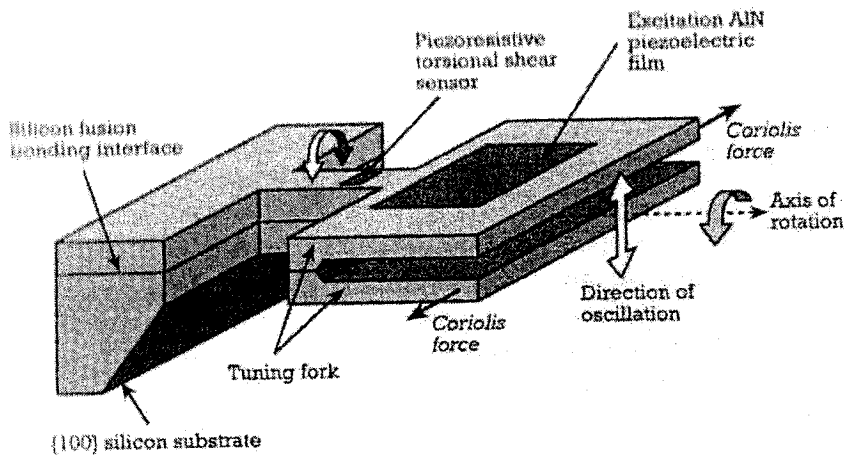

Fig. 4.9 Beam-plate type angular-rate sensor under rotation [34]

Assume stiffness of tire is constant. Tire pressure is expressed by:

$$P = \frac{nRT}{V} \tag{4.8}$$

where V is the air volume which is also random due to randomness of tire vertical relative displacement. The temperature T is assumed to be constant. Extend (4.8) into Taylor series, and neglect high order items,

$$P + \Delta P = P + (-\frac{nRT}{V^2}\Delta V) \tag{4.9}$$

Therefore, dynamic component of pressure is expressed by,

$$\Delta P = -\frac{nRT}{V^2}\Delta V \tag{4.10}$$

Figure 4.10 shows the approximated graph of a tire and its deformation. The deformation part of tire is expressed by the shaded area schematically.

Area of shaded part in Figure 4.10 is given by,

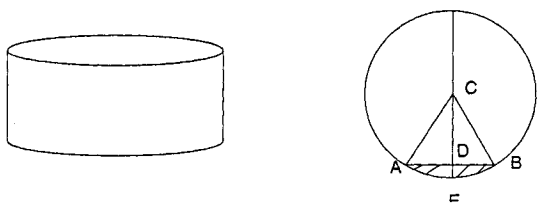

Fig. 4.10 Tire under random displacement

$$A = R_1^2 \left(\theta - \frac{\sin(2\theta)}{2} \right) \tag{4.11}$$

where $\theta = \angle ACD$, and volume determined by shaded area is given by,

$$V = R_1^2 \, H \left(\theta - \frac{\sin(2\theta)}{2} \right) \tag{4.12}$$

where H is tire width and R_1 is tire outer radius. Thus, the changing in volume with

$$\Delta V = R_1^2 H \left(1 - \cos(2\theta)\right) \Delta\theta \tag{4.13}$$

$$\cos\theta = \frac{R_1 - Z}{R_1} = 1 - \frac{Z}{R_1} \tag{4.14}$$

$$\sin^2\theta = 2\frac{Z}{R_1}\left(1 - \frac{Z}{R_1}\right) \approx 2\frac{Z}{R_1} \tag{4.15}$$

where $Z = DE$ in Figure 4.10. Differentiate equation (4.14)

$$(\sin\theta)\Delta\theta = \frac{1}{R_1}\Delta Z \tag{4.16}$$

Substitute equations (4.15) and (4.16) into equation (4.13)

$$\Delta V = R_1^2 H (2\sin^2\theta)\Delta\theta$$

$$= R_1^2 H 4 \frac{Z}{R_1} \frac{\Delta Z}{R_1 \sin\theta} = 4HZ\Delta Z\sqrt{\frac{R_1}{2Z}}$$

$$\Delta V = 2\sqrt{2R_1 Z}\; H\Delta Z \tag{4.17}$$

Substitute equation (4.17) into equation (4.10), finally,

$$\Delta P = -\frac{P}{V} 2\sqrt{2R_1 Z}\; H\Delta Z \tag{4.18}$$

The relationship between tire pressure spectral density function and relative displacement spectral density function is,

$$S_{\Delta P}(\omega) = (\frac{8R_1P^2}{V^2} H^2 Z) S_{\Delta Z}(\omega) \tag{4.19}$$

where, Z is static displacement due to the vehicle's weight, and P and V are initial pressure and volume, respectively, and $S_{\Delta Z}(\omega)$ is actually $S_{Z_1}(\omega)$ which has been stated in detail in Section 4.1.1. With the Equations (4.19), (4.4) vehicle structure and its velocity, and type of road profile, the spectral density tire pressure can be obtained.

4.2 MEMS Structures and Modeling

A complete MEMS is a complex system which is difficult to analyze. In general, the structural components of MEMS consist of simple beam and plate type of structures as can be realized from Figures 4.6 to 4.9.

The accelerometer in Figure 4.8 or angular-rate sensor in Figure 4.9 may be modeled efficiently as one-degree-of-freedom system. Beams can be modeled as springs in general (including torsion spring), and the plate can be modeled as a rigid body with proof mass as shown in Figure 4.11.

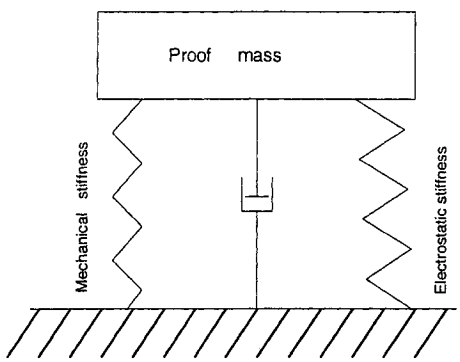

Fig. 4.11 Schematic model of beam-plate capacitive sensor

MEMS structure shown in Figures 4.6, 4.7 can be modeled as beam-plate and (or) plate-plate structures depending upon the relative stiffness of the plate element with reference to the beam element. If the MEMS structures shown in Figure 4.6 and 4.7 are modeled as a beam-plate, and the stiffness of the plate is far greater than that of the beam, then the MEMS structure may be simplified to a flexible beam with end attached rigid plate as shown in Figure 4.12.

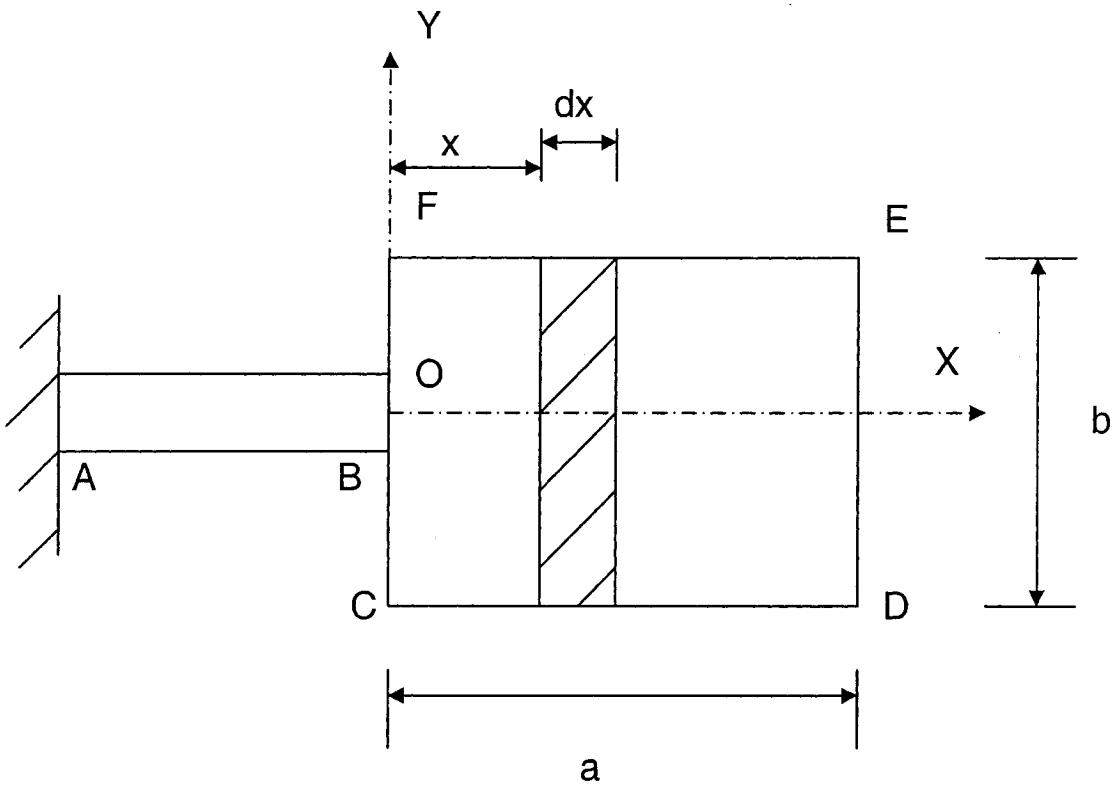

Fig.4.12 Schematic structure of beam-plate type pressure sensor

Discretizing the plane beam AB into N-1 elements (N nodes), then the system would have $2N$ *DOF* described by $\{v_1, v_2, \ldots\ldots v_{2N-1}, v_{2N}\}$, where v_{2i-1} is vertical displacement and

v_{2i} is rotation. Thus, the stiffness and mass of the beam are $2N \times 2N$ matrices which may be written as:

$$K_{BEAM} = \begin{bmatrix} k_{11} & & k_{1(2N)} \\ . & & \\ . & & \\ . & & \\ k_{(2N)1} & & k_{(2N)(2N)} \end{bmatrix} \tag{4.20}$$

$$M_{BEAM} = \begin{bmatrix} m_{11} & & m_{1(2N)} \\ . & & \\ . & & \\ . & & \\ m_{(2N)1} & & m_{(2N)(2N)} \end{bmatrix} \tag{4.21}$$

Since the plate is treated as a rigid body, the kinetic energy of the plate can be given by,

$$T = \frac{1}{2} \iint_{CDEF} \rho h dA \left(\dot{v}_{2N-1} + x \dot{v}_{2N} \right)^2 = \frac{\rho h}{2} \left(ab \dot{v}_{2N-1}^2 + \frac{1}{3} a^3 b \dot{v}_{2N}^2 + a^2 b \dot{v}_{2N} \dot{v}_{2N-1} \right) \tag{4.22}$$

where h and ρ are thickness and density of the plate, respectively. Considering Eq. (4.22) and the methodology explained in Chapter 2, the mass matrix of whole structure is given by:

$$M = \begin{bmatrix} m_{11} & & m_{1(2N)} \\ . & & \\ . & & \\ . & & \\ m_{(2N)1} & & m_{(2N)(2N)} \end{bmatrix} +$$

$$\begin{bmatrix} 0 \; . \; . \; . & 0 & 0 \\ . & & \\ . & & \\ . & & \\ 0 & \rho hab & \frac{1}{2}\rho ha^2 b \\ 0 & \frac{1}{2}\rho ha^2 b & \left(\frac{1}{3}\rho ha^3 b\right) \end{bmatrix}_{2N\times 2N} =$$

$$\begin{bmatrix} m_{11} \; . \; . \; . & & m_{1,2N} \\ . & & \\ . & & \\ . & & \\ m_{2N-1,1} & (m_{2N-1,2N-1} + \rho hab), & (m_{2N-1,2N} + \frac{1}{2}\rho ha^2 b) \\ m_{2N,1} & (m_{2N,2N-1} + \frac{1}{2}\rho ha^2 b), & \left(m_{2N,2N} + \frac{1}{3}\rho ha^3 b\right) \end{bmatrix}_{2N\times 2N} \tag{4.23}$$

Compared to the strain energy of the beam, the potential energy due to the weight of the system is very small. Thus, the stiffness of the whole structure is assumed to be the same as that of the beam. Using virtual work principle, the equivalent nodal force of the whole structure may be described as:

$$\{F\}^T = \{f_1, f_2, \; . \; . \; . \; f_{2N-1} \; f_{2N}\} + \left\{0, \; 0, \ldots, pab, \frac{1}{2}pa^2 b\right\}_{1\times 2N}$$

$$= \left\{f_1, f_2, \; . \; . \; . \; f_{2N-1} + pab \; , f_{2N} + \frac{1}{2}pa^2 b\right\} \tag{4.24}$$

where $\{f_1, f_2, \; . \; . \; . \; f_{2N-1} \; f_{2N}\}$ is the vector of equivalent nodal force in the beam which is the null vector for the present study and p is the pressure which is sensed by the

rigid plate. With the mass and stiffness matrix of the MEMS structure given by Eqn. (4.20) and (4.23), and the equivalent nodal force expressed in Eq.(4.24), the equation of motion regarding MEMS structure can be established. Therefore, the dynamic performances of MEMS structure can be predicted if the nature of pressure p is known.

4.3 Design Issues and Reliability of MEMS

When MEMS structure is under random environment, the responses of the structure including stress are therefore random. In such situation, the "three-sigma" design criterion is typically used to design structures where brittle fracture or fatigues are not considered to be the principal failure modes. A basic requirement commonly employed in MEMS design criteria documents is that, for a safe design [8]:

$$R \geq 3\sigma_S \tag{4.25}$$

where R is material strength and σ_s is the standard deviation of the stress. The implication is that mean stress μ_s is zero and strength R is deterministic. Because process S is Gaussian, the probability that stress will exceed three times its RMS value is

$$P[|S(t)|] \geq 3\sigma_s = 0.0026 \tag{4.26}$$

When $R = 3\sigma_s$, the probability of stress exceeding the strength can be considered to be 0.3%. In reality, the mean stress is not zero and material strength is a random

variable. For this more general case a basic criterion for a safe design under no mean stress conditions can be written as

$$\mu_R \geq \xi \sigma_s \tag{4.27}$$

where μ_R is the mean value of the strength, R, and the factor ξ is function of μ_s / σ_s and the coefficient of variation of R, $C_R = \sigma_R / \mu_R$. The function ξ has been derived by numerical analysis and the results are shown in Figure 4.13 [8].

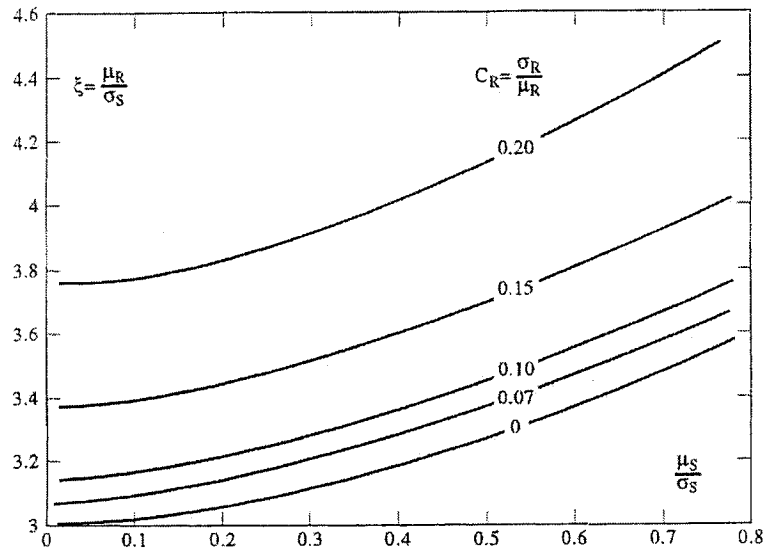

Fig. 4.13 Generalized three-sigma criterion [8]

Another important effect of random environment on MEMS structure is its reliability. Figure 4.14 is a schematic of a capacitive inertial sensor. While parallel plate capacitors have good actuation and sensing abilities, they have some severe limitations. One of the limitations in these devices is the potential of the plate pull-in. In MEMS

structure, when the two metal surfaces come into contact, adhesive forces exert a strong bond that usually causes failure. This problem is especially prevalent in parallel plate devices because the elastic force increases non-linearly with distance. A common convention in design rule used is that, if $\Delta x \geq \frac{1}{3}d$, the device will be pulled-in. To prevent this, parallel plate devices under random environment must be designed to displace much less this amount due to random loading and excitation.

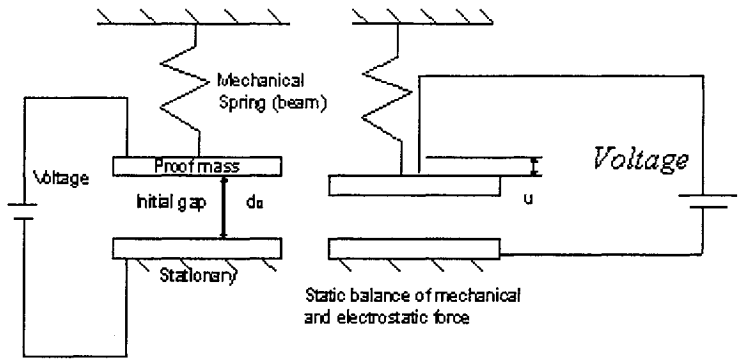

Fig. 4.14 Schematic of a capacitive sensor

4.4 Application to MEMS Structure

Design problems and reliability of MEMS in stochastic environment will be discussed in this section.

4.4.1 Design problem of MEMS structure in random environment

As an example, design of a piezoresistive tire pressure device which is subjected to random tire pressure will be developed in the following case.

MEMS structure is shown in Figure 4.15. The dimensions, the material characteristics and the load condition of the plate are as follows:

Width: 100 μm, Length: 100 μm, Thickness: 8 μm, Density: 2300 kg/m^3, Young's modulus: 73 Gpa, Possion's ratio: 0.17, Yielding strength: 700 MPa. Damping coefficients of all modes are assumed to be 0.02. Excitation is spatial uniform random pressure and its power spectral density function is shown in Figure 4.16 and static tire pressure is 3.5×10^5 Pa.

The following are the solutions along with discussion:

1) Using finite element method of bending thin plate which has been explained in Chapter 2, the motion equations of the MEMS flexural plate can be set up.

2) Since the random characterization of the measurement (pressure) is given and the random response of multi-degree-of-freedom system to random input can be obtained as described in Chapter3, thus the cross spectral density function and covariance of the nodal displacement response $\{x\}$ can be computed directly or using normal mode summation technique. The computational model has been presented in detail in Section 3.7, and has been verified with a simple discrete 2-degree-of-freedom system in Section 3.9.

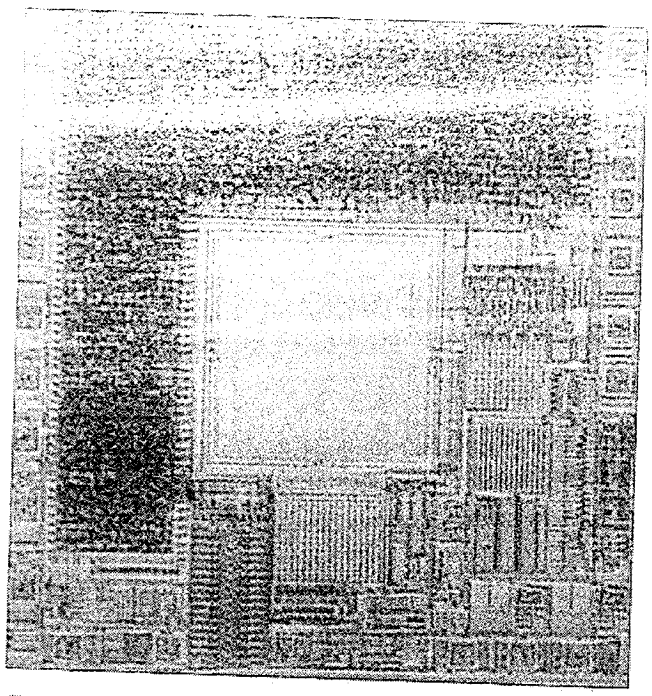

Fig. 4.15 Photomicrograph of piezeresistive pressure sensor, the sensor area is the square in the center of the chip [21]

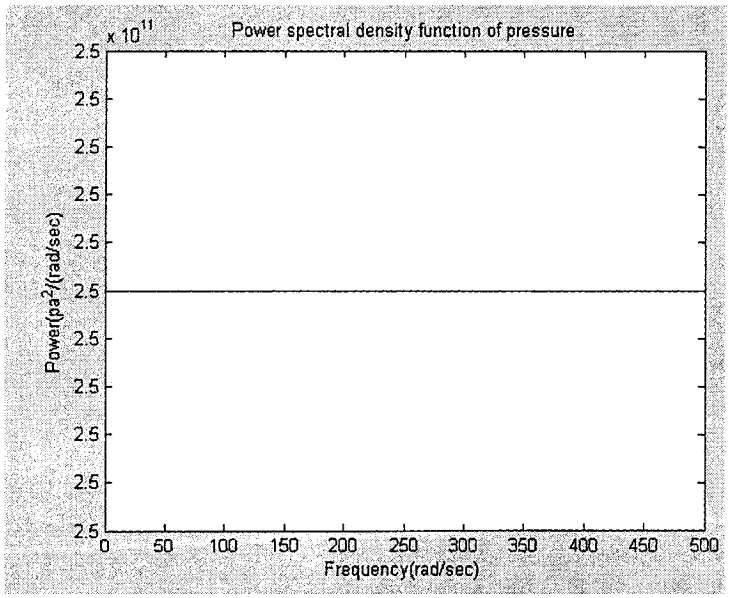

Fig. 4.16 Power spectral density function of pressure

3) All performances of the considered structure are based on the nodal displacements. Since the dynamic characterization of the nodal displacement response $\{x\}$can be obtained, the randomness of strain, stress can then be obtained subsequently. For design problem, covariance of the maximum stress is the main interest.

4) Covariance of maximum stress of the MEMS plate in this study is $\begin{bmatrix} 2.8117 & 0.8435 & -0.1544 \\ 0.8435 & 0.2531 & -0.046 \\ -0.1544 & -0.0463 & 0.0085 \end{bmatrix} \times 10^{15}(Pa)^2$. It is the covariance of stress tensor $\begin{Bmatrix} \sigma_x \\ \sigma_y \\ \tau_{xy} \end{Bmatrix}$ at the center point of the side. The diagonal terms are variances of $\sigma_x, \sigma_y, \tau_{xy}$ respectively. Thus the standard deviation of $\sigma_x, \sigma_y, \tau_{xy}$ may be written as: $\delta_{\sigma_x} = \sqrt{2.8117 \times 10^{15}}\, pa = 53 MPa$, $\delta_{\sigma_y} = \sqrt{0.2531 \times 10^{15}}\, pa = 5.1 MPa$, $\delta_{\tau_{xy}} = \sqrt{0.0085 \times 10^{15}}\, pa = 0.92 MPa$.

Thus, the value of 3-sigma is 159 MPa. The mean maximum stress due to static pressure is 71 MPa

5) According to different MEMS environment, there will be different dynamic performance. These performance results are very useful for MEMS design. For example, in this case, the yielding of this material is 700 *MPa*, which is far greater than 3-sigma value of maximum stress. Therefore, the design of MEMS structure in the stochastic environment shown in Figure 4.15 is safe enough.

4.4.2 Reliability analysis

A typical MEMS structure shown in Figure 4.7 with its schematic figure shown in Figure 4.12 is considered here for a case study. It is assumed that the structure is subjected to a random base excitation in aerospace application. The input spectral density function is demonstrated in Figure 4.5. The dimensions of the structure are: width of plate: $100\,\mu m$, length of plate: $100\,\mu m$, length of AB: $100\,um$, width of AB:$10\ um$, thickness: $5\ \mu m$. The density and the Young's modulus are $2300\,kg/m^3$ and 73 GPa, respectively and the Possion's ratio is 0.17. The mode damping coefficient is assumed to be 0.02.

The solutions are discussed below:

1) The structure is the combination of beam and rigid plate. The modeling of this type of structure has been presented in Section 4.2. Let us rewrite the mass matrix given in Eq. (4.23):

$$M = \begin{bmatrix} m_{11} & \cdots & & m_{1,2N} \\ \vdots & & & \\ m_{2N-1,1} & & (m_{2N-1,2N-1} + \rho hab), & (m_{2N-1,2N} + \frac{1}{2}\rho ha^2 b) \\ m_{2N,1} & & (m_{2N,2N-1} + \frac{1}{2}\rho ha^2 b), & \left(m_{2N,2N} + \frac{1}{3}\rho ha^3 b\right) \end{bmatrix}_{2N\times 2N}$$

The total kinetic energy of the structure can be written as,

$$T=\frac{1}{2}[v,x_1,x_2,\ldots x_{2N}]\begin{bmatrix} mt_{11}, & mt_{12} \ldots & mt_{1,(2N+1)} \\ mt_{21} & & \\ mt_{31} & & \\ \cdot & & \\ \cdot & & \\ mt_{(2N+1),1} & & \end{bmatrix}\begin{bmatrix} v \\ x_1 \\ x_2 \\ \cdot \\ \cdot \\ \cdot \\ x_{2N} \end{bmatrix} \quad (4.28)$$

where $x_1, x_2, \ldots x_{2N}$ are desired nodal displacements, v is base excitation. mt_{ij}, m_{ij} are terms of mass matrix after assembling.

2) Now recalling the finite element modeling of continuous structure excited by base motion explained in Section 3.8, the equation of motion can be written as,

$$[M]_{2N\times 2N}\left\{\ddot{x}\right\}_{N\times 1}+[K]_{2N\times 2N}\{x\}_{N\times 1}=-\begin{Bmatrix} mt_{21}\ddot{v}+kt_{21}v \\ mt_{31}\ddot{v}+kt_{31}v \\ \cdot \\ \cdot \\ \cdot \\ mt_{(2N+1),1}\ddot{v}+kt_{(2N+1),1}v \end{Bmatrix} \quad (4.29)$$

Since the interest in this case study is the gap of the two plates, namely, $z_{N-1}=x_{N-1}-v$, it is necessary to replace $\{x\}$ by z. Setting $\{z\}=\{x\}-\{0,0,\ldots,v,0\}^T$ the equation of motion of the structure can be reformatted as:

$$[M]_{2N\times 2N}\left\{\ddot{z}\right\}_{N\times 1}+[C]\left\{\dot{z}\right\}+[K]_{2N\times 2N}\{z\}_{N\times 1}=-\{F\} \quad (4.30)$$

where

$$F = -\begin{Bmatrix} mt_{21}\ddot{v} + kt_{21}v & + m_{1(2N-1)}\ddot{v} + k_{1(2N-1)}v + c_{1(2N-1)}\dot{v} \\ mt_{22}\ddot{v} + kt_{22}v & + m_{2(2N-1)}\ddot{v} + k_{2(2N-1)}v + c_{2(2N-1)}\dot{v} \\ \cdot & \\ \cdot & \\ \cdot & \\ mt_{(2N+1),1}\ddot{v} + kt_{(2N+1),1}v + m_{2N(2N-1)}\ddot{v} + k_{2N(2N-1)}\dot{v} + c_{2N(2N-1)}\dot{v} \end{Bmatrix} \tag{4.31}$$

3) Because the random base excitation v is known, the spectral density function of generalized force vector in left side of equation can be obtained. Thus, the response characterization can then be obtained.

4) The covariance of $\begin{Bmatrix} z_{2N-1} \\ z_{2N} \end{Bmatrix}$ is

$$\delta = \begin{bmatrix} 1.1215\times10^{-11} & 1.94\times10^{-7} \\ 1.94\times10^{-7} & 0.0034 \end{bmatrix} \tag{4.32}$$

where z_{2N-1} is the relative displacement, and z_{2N} is rotation. Thus, the gap standard deviation is $\sqrt{1.1215\times10^{-11}} = 3.3\mu m$

The probability of failure can be estimated for different initial gap. Thus the above prediction will be helpful in avoiding the failure of the device due to snapping under random excitation.

CHAPTER 5

TESTING OF MEMS STRUCTURES UNDER RANDOM ENVIRONMET

5.1 Introduction

Performance response modeling of multi degree-of-freedom system under random environments has been developed and verified in Chapter 3. Meanwhile, finite element modeling of continuous structure under random base excitation and micromechanical structures has also been presented in Chapters 3 and 4, respectively. In this chapter, a test of MEMS structure under random excitation is demonstrated to verify the finite element modeling.

5.2 Testing of MEMS Structures

A simple cantilever type of MEMS structure is tested. Atomic force microscope (AFM) probes are chosen for testing. A sample of such probes is given in Figure 5.1, and the dimensions of the tested AFM cantilever are provided in Table 5.1.

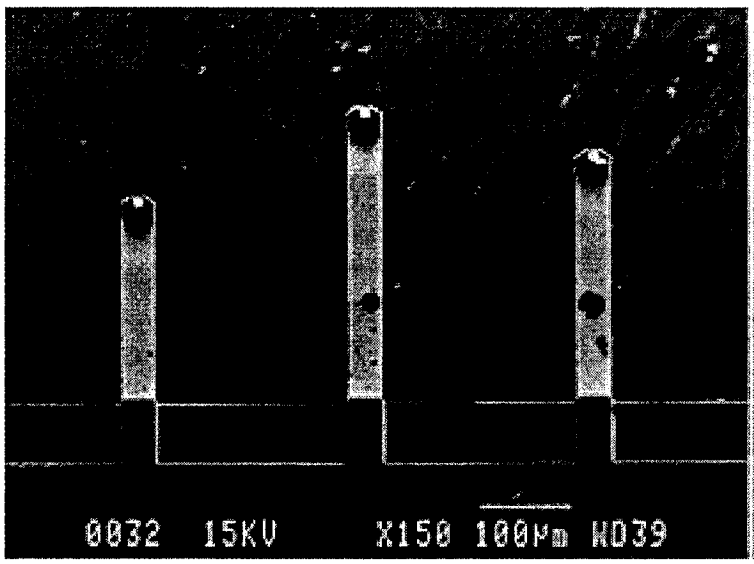

Fig. 5.1 An SEM photo of AFM type cantilevers used in this study [33]

Table 5.1 The dimension of the AFM cantilevers used in the test

Cantilever A	Length	Width	Thickness	Fundamental frequency
	351 microns	34.8 microns	1.61 microns	18000Hz

This bimorph microcantilevers are made up of silicon layer and a thin aluminum layer on top side. The aluminum coating has reflection characteristics that allow for excellent testing suitability with a HeNe laser (91% reflection at 632 nm) with virtually no reduction in signal in sensing from the cantilever surface.

For this experimentation, a non-contact method, Laser Doppler Velocitimetry [33] is adopted to measure the dynamic response of the cantilevers. The test equipment used in these experiments comprised a helium-neon laser, some simple focusing optics for beam shaping and laser spot size optimization and an acoustic system to provide the base excitation energy.

A flat-face acoustic speaker was selected for the ease of mounting, and test structures. The output signal analysis was done with an oscilloscope for the time-domain analysis, and a frequency analyzer with an integrated signal generator for the frequency-domain. Interpretation, analysis and cross referencing of these signals to a single tone input signal (2kHz sinusoidal with appropriate amplitude) provided the basis for proper experimental set-up (axial and radial alignment, lens alignment, laser beam focusing, acoustic signal amplitude, signal sensitivity, etc.). Higher single tone frequencies (>15kHz) were more sensitive to apparatus misalignments due to the inherent reduction in signal amplitude, and therefore, were used to "fine tune" the experimental set-up before device testing was undertaken.

The HeNe laser was mounted onto a fixed immovable platform. All other equipment was aligned with respect to the laser position. Both lenses, one diverging the other converging respectively, were mounted onto individual XY micro-positioners,

while the flat-face was mounted onto a rotational platform fastened onto a XYZ micro-positioner. Pitch misalignment was corrected by the insertion of an appropriate wedge device at the base of the speaker. The schematic of the experimental set up is shown in Figure 5.2.

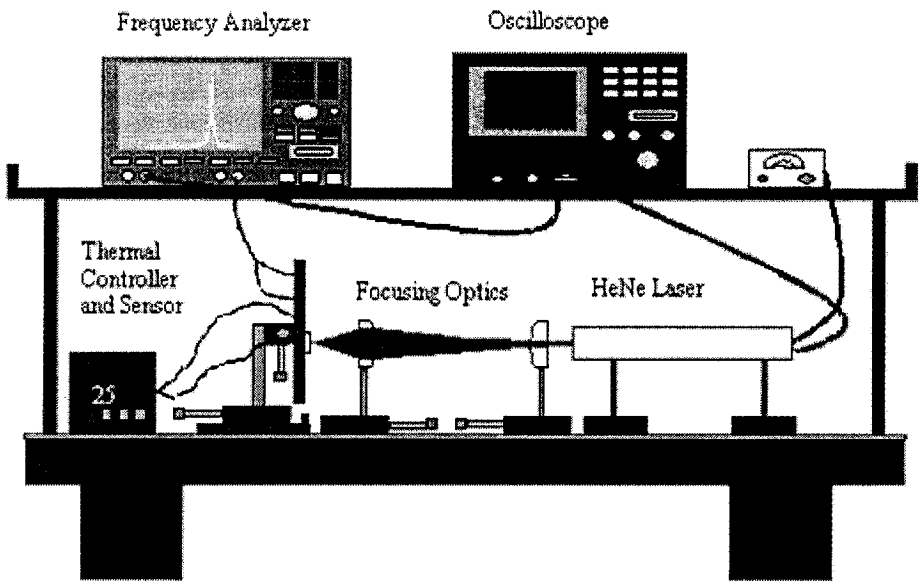

Fig. 5.2: Overview of the experimental set-up[33]

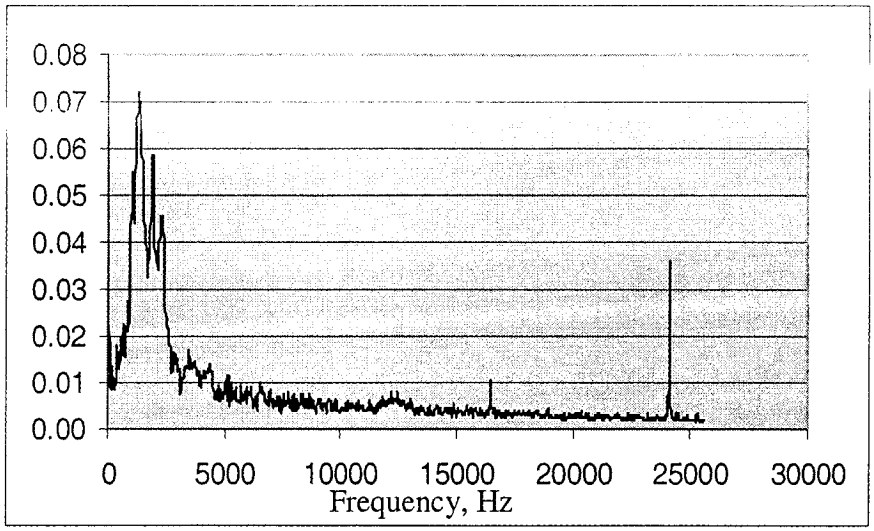

Fig. 5.3: Displacement response of the substrate

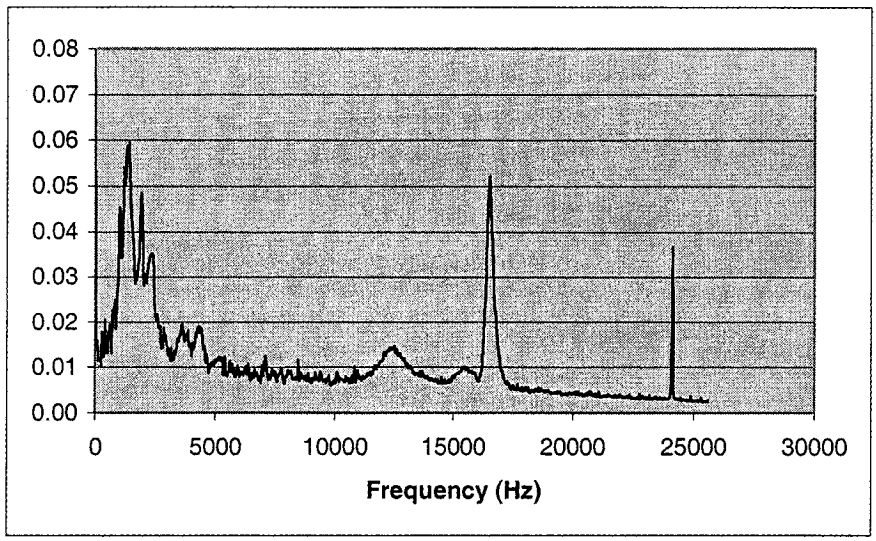

Fig. 5.4 Displacement response of the cantilever tip

Initial tuning of the setup is important for testing. Once a proper single response was obtained from the substrate surface of the AFM chip, the laser was focused onto one of the AFM cantilevers.

The whole device was excited by random base excitation which was generated by Frequency Analyzer The input excitation was the band pass between the frequencies 20Hz to 20kHz. As a result, the responses of the substrate and the tip of the cantilever are also random. Figure 5.3 and Figure 5.4 show the responses of the substrate and the beam tip respectively. Actually, the transform function of a structure is determined only by the structure and its boundary conditions, and the type of the excitation makes no effect on the transform function (irrespective of sinusoid or random excitation). The purpose of this test is to verify the finite element modeling of the continuous structure excited by base excitation through comparison the gain functions obtained analytically and experimentally. After the tip response shown in Figure 5.4 is divided by that of the substrate shown in Figure 5.3, the gain function of the cantilever can be obtained, which is shown in Figure5.5.

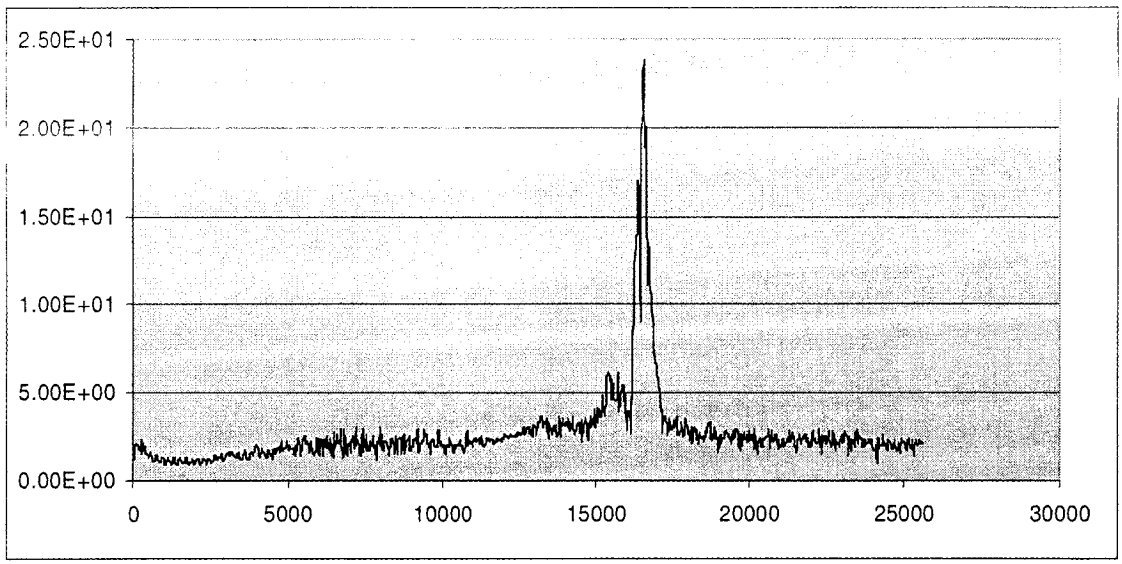

Fig. 5.5 Gain function of the micro-cantilever. This function is measured on the condition of that the AFM device was subjected to random base excitation

5.3 Comparison and Discussion

In this section, the analytical transform and gain function between the tip response and base excitation will be presented using the model proposed in Chapter 3. Furthermore, this analytical result will be compared to the testing result given in Figure 5.5.

The considered cantilever beam is a continuous structure, in order to study the dynamic performance of this structure excited by base motion, the finite element method has to be employed. Thus the motion of equation of this structure can be given as

$$[M]\{\ddot{x}\}+[C]\{\dot{x}\}+[K]\{x\}=\{F\} \tag{5.1}$$

where $[M]$,$[C]$, $[K]$ are mass, damping , and stiffness matrices respectively, $\{F\}$ is equivalent generalized nodal force due to base excitation, and $\{x\}$is nodal displacements

response of the structure.

Using the modeling proposed in Section 3.8 and Equation (3.41), the equivalent nodal force $\{F\}$can be defined as:

$$\{F\} = -\begin{Bmatrix} \frac{1}{2}(m_{12}+m_{21})\ddot{v} + \frac{1}{2}(k_{12}+k_{21})v \\ \frac{1}{2}(m_{13}+m_{31})\ddot{v} + \frac{1}{2}(k_{13}+k_{31})v \\ \frac{1}{2}(m_{14}+m_{41})\ddot{v} + \frac{1}{2}(k_{14}+k_{41})v \\ . \\ , \\ \frac{1}{2}(m_{1N}+m_{N1})\ddot{v} + \frac{1}{2}(k_{1N}+k_{N1})v \end{Bmatrix} \tag{5.2}$$

where m_{ij} and k_{ij} are the terms in the unmodified mass and stiffness matrix $[m],[k]$which are used to express total kinetic and potential energy of the whole structure, N is number of the freedom of the system including the known freedom (base excitation) , N -1 is the number of degrees-of-freedom of the structure which need to be solved, v is base displacement, and $\ddot{v}$ is base acceleration.

Using Normal Mode Method which has been discussed in detail in Chapter 3, the coupled differential equations in (5.1) can be a group of uncoupled differential equations which is given by equation (5.3).

$$[\phi]^T[M][\phi]\{\ddot{q}\} + [\phi]^T[C][\phi]\{\dot{q}\} + [\phi]^T[K][\phi]\{q\} = [\phi]^T\{F\} \tag{5.3}$$

where $[\phi]$ is modal matrix , $\{q\}$is modal coordinates, $\{Q\}$is modal force, and $\{x\}=[\phi]\{q\}$

$$\{Q\}=[\phi]^T\{F\} \tag{5.4}$$

Thus, the Equation(5.3) can be written as (5.5)

$$\left[\bar{M}\right]\left\{\ddot{q}\right\}+\left[\bar{C}\right]\left\{\dot{q}\right\}+\left[\bar{K}\right]\{q\}=\{Q\} \tag{5.5}$$

where

$$\left[\bar{M}\right]=[\phi]^T[M][\phi] \qquad \left[\bar{C}\right]=[\phi]^T[C][\phi] \qquad \left[\bar{K}\right]=[\phi]^T[K][\phi] \quad , \tag{5.6}$$

and they are diagonal.

Hence

$$\{q\}=[H(\omega)]\{Q\}=[H(\omega)][\phi]^T\{F\} \tag{5.7}$$

where the transform function matrix $[H(\omega)]$ is diagonal,

$$[H(\omega)]=\begin{bmatrix} H_1(\omega) & 0 & 0\ .\ .\ . & 0 \\ 0 & H_2(\omega) & 0.\ .\ . & 0 \\ . & & & \\ . & & & \\ 0, & 0, & 0,\ .\ .\ . & H_{N-1}(\omega) \end{bmatrix}_{(N-1)\times(N-1)} \tag{5.8}$$

and $H_j(\omega)=\dfrac{1}{M_j(\omega_j^2-\omega^2+2i\xi_j\omega\omega_j)}$ is the j^{th} modal transform function, ω_j is the j^{th} undamped natural frequency, M_j is the j^{th} modal mass, and ξ_j damping ratio of mode j.

Pre-multiply Eq.(5.7) with $[\phi]$

$$[\phi][q]=\{x\}_{N-1}=[\phi][H(\omega)][\phi]^T\{F\} \tag{5.9}$$

The fundamental frequency of the micro-beam is 18000 Hz. The mode coordinates can be simplified as,

$$\{x\}=[\phi]\{q_1\} \tag{5.10}$$

On rewriting Eq.(5.9),

$$\begin{Bmatrix} x_1 \\ x_2 \\ . \\ . \\ x_{N-2} \\ x_{N-1} \end{Bmatrix}_{N-1} = \begin{bmatrix} \phi_{11} \\ \phi_{12} \\ . \\ . \\ . \\ \phi_{N-1} \end{bmatrix} H_1(\omega)[\phi_{11}\ \phi_{12}\ .\ .\ .\ \phi_{N-1}] \begin{Bmatrix} m_{12}\omega^2+k_{12} \\ m_{13}\omega^2+k_{13} \\ . \\ . \\ m_{1N}\omega^2+k_{1N} \end{Bmatrix}_{N-1} \{v\} \tag{5.11}$$

Thus

$$\left\{\frac{x_1}{v},\frac{x_2}{v},\ .\ .\ .\ \frac{x_{N-2}}{v},\frac{x_{N-1}}{v}\right\}^T = h_{1j}\quad j=1,(N-1) \tag{5.12}$$

$$h_{1j}=\left(\sum_{i=1}^{N-1}\phi_{1j}\phi_{1i}\left(m_{1(i+1)}\omega^2-k_{1(i+1)}\right)\right)H_1(\omega) \tag{5.13}$$

where h_{1j} is the transform function of the response between j^{th} degree-of-freedom and base excitation v, x_{N-2} is the vertical displacement of the beam tip, x_{N-1} is the rotation of the beam tip.

The desired transform function is $h_{1(N-2)}=\frac{x_{N-2}}{x}$. The cantilever geometries were measured using an optical microscope and are in agreement with the dimensions supplied by the manufacturer. The dimensions of the cantilevers are given in Table 5.1. Since

aluminum layer is very thin compared with that of silicon, for the theoretical analysis the value for Young's modulus was taken as 170Gpa, and the density for silicon was taken as 2332kg/m^3.

Using equation (5.13) and data in Table 5.1, analytical gain function $|h_{1(N-2)}|$ between tip displacement and base excitation can be obtained. When all mode damping ratios are assumed as to be typically 0.02, the result is shown in Figure 5.6.

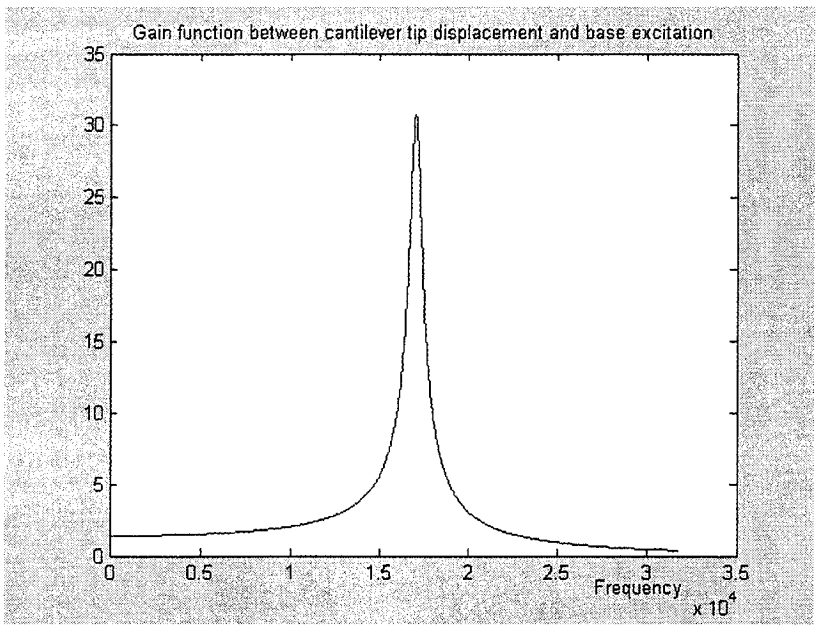

Fig. 5.6 Gain function between cantilever tip displacement and base excitation ($\xi = 0.02$)

Compare the testing results shown in Fig.5.5 and the theoretical results given in Fig. 5.6, it can be realized that good agreement exists between the experimental and

analytical results. Thus it can be concluded that the finite element modeling of continuous structure excited by base motion developed in Chapter 3 can efficiently and accurately predict the dynamic response of MEMS structures in random environment.

CHAPTER 6

CONCLUSIONS

This thesis attempted modeling and testing MEMS structures that could be subjected to stochastic working environment which might be random external force or random base excitation. The author has modeled MEMS structure and built equations of motion with Hamilton's principle, Lagrange's equations, and finite element method to explore dynamic performance, design issue and reliability of MEMS in such environment. In order to simplify equations of motion of the structure, normal mode method has been adopted. Furthermore, since fundamental frequency of MEMS structure is very high compared to excitation frequency, summation method was used to reduce the size of motion equations according to the excitation frequency. This technique makes it possible to compute response of MEMS structure fast and effectively.

According to general nodal force which is caused by random measurements or random base acceleration, cross spectral density function of input can be obtained. Direct method and indirect method were both used to derive displacement response formula. The proposed dynamic models can be applied to both design and reliability of MEMS structures.

The response of multi-degree-of-freedom system excited by random force has been studied in detail. The formulation proposed in the thesis is found to be in good agreement with other published results and experiments. Moreover, dynamic models of continuous structure which are subjected to base (acceleration, velocity, or displacement) excitation have also been studied and verified in this thesis.

Using the present formulation, any beam-plate type MEMS structures under bending can also be modeled easily.

To finally conclude, this thesis provides some guidelines for design of beam-plate type of MEMS structures and reliability analysis of MEMS structures under random environment.

References

1. B. Stark, "MEMS reliability assurance guidelines for space aApplication, Jet propulsion laboratory", California, National Aeronautics and Space Administration, January ,1999.

2. D. Nathanson , J. Leonard "The resonant gate transistor", IEEE Transactions on Electron Devices, March, 1967

3. H. Helvajian, S. W. Janson, "Microengineering technology for space systems", The Aerospace corporation report, September 30,1995.

4. N. MacDonald, "Microelectromechanical systems", EE493, January 18,1997

5. M. Petyt , "Introduction to finite element vibration analysis", Cambridge University Press, 1990.

6. D. J. Gorman, "Free vibration analysis of rectangular plates", Elsevier North Holland, Inc. 1982

7. M. Mukhopadhyay, "Finite element free flexural vibration analysis of arbitrary plates", 1998 Elsevier Science B.V.

8. P. H. Wirsching, T. L. Paez, K. Ortiz, "Random vibration, Theory and Practice", John Wiley & Sons,1995.

9. J. B. Roberts, P. D. Spanos, "Random vibration and statistical linearication", Wiley,1990, New York.

10. H.C. Stephen, D.William, "Random vibration in mechanical systems", Acadenmic press, 1963, New York.

11. Ray W. Clough, J. P. Penizen,"Dynamics of structures", McGraw-Hill,1975, New York.

12. M. W. Bonilha, "Analysis of the spatial response distribution of the bending wave field generated by the random vibration of thin plate-like structural components", Journal of Dynamic Systems, Measurement , and Control, 1997, Vol.117, pp541-546

13. R. S. Harichandran, "Random vibration under propagating Excitation: Closed-form solutions", Journal of Engineering Mechanics, Vol.117, No.7, September,1995.

14. R. S. Harichandran, "Random vibration of laminated FRP plates with material nonlinearity using high-order shear theory", Journal of Engineering Mechanics, Vol. 125, September, 1999, pp575-586.

15. T. A. Core, "Fabrication Technology for an Integrated Surface-Micromachined Sensor", Solid State Technology, October, 1996, October,1996.

16. W. C. Tang, "MEMS applications in space exploration, Micromachined devices and components III", Proc. SPIE, Vol. 3224, September, 1997, pp197-202.

17. D. M. Tanner, "MEMS reliability in a vibration environment", IEEE International Reliability Physics Symposium, San Jose, CA, April 10-13, 2000, pp139-145

18. W. J. Brown, B. Stuart, "Reliability and Fatigue Testing of MEM, Tribology Issues and Opportunities in MEMS", November 9-11,1997, Klewer Academic Publications.

19. D. G., McIntyre, S. J. Cunningham, T. S. Carper, P. D. Jaramillo, "Characterization of the influence of fabrication methods on microstructure failure", Sensor and Actuators, Vol. A 60, 1997, pp 181-185.

20. G. X. Li, F. A. Shemansky , "Drop test and analysis on micromachined structures", Sensors and Actuators, Vol. A85, 2000, pp.280-286.

21. J. K. Reynold, D. Catling, R. C. Blue, N. I. Maluf, T. Kenny, "Packaging a piezoresistive pressure sensor to measure low absolute pressures over a wide sub-zero temperature range", Sensors and Actuators, Vol. A83, 2000, pp 142-149.

22. B. R. Davies, V. I. Bateman, F. A. Brown, S. Montague, T. R. Murray, "Micromachined accelerometer design, modeling and validation", Proc. Conf. Modeling Simulation Microsyst., Santa Clara, CA, April 1998, pp. 552-556.

23. M. D. Tanner, M. Danelle, "MEMS reliability in shock environments", Proc. IEEE Int. Reliability Physics Symp., San Jose, CA, April 2000, pp.129-138.

24. A. Beliveau, G. T. Spencer, K. A. Thomas, and S. L. Roberson, "Evaluation of MEMS Capacitive accelerometers", IEEE Design Test Computation, 1999, pp.48-56, October.

25. A. Hartzell, D. Woodilla, "Reliability methodology for prediction of micromachined accelerometer stiction", Proc. IEEE Int. Reliability Physics Symp., San Diego, CA, Mar. 1999, pp. 202-205.

26. Srikar et al., "The reliability of Microelectromechanical systems in shock environments", Journal of Microelectromechanical systems, Vol. 11, June, 2002, pp206-214.

27. G. X. Li, D. N. Koury "Modeling and experimental observation of drop testing of micro-machined structures", Eurosensors XIII, 1999, The Hague, The Netherlands.

28. U. Wagner, J. Franz, and M. Schweiker, W. Bernhard, R. Muller-Fiedler, B. Michel, O. Paul,"Mechanical reliability of MEMS structures under shock load, Microelectronics Reliability", Vol. 41, 2001, pp. 1657-1662.

29. D. M. Tanner "MEMS reliability: test structures, experiments and failure modes", Sandia Report. USA, 2000.

30. W. M. Spengen., "MEMS reliability from a failure mechanisms perspective, Microelectronics Reliability", Vol. 43, 2003, pp1049-1060.

31. S. Lu, "Optimum design of "road-friendly" vehicle suspension systems subjected to rough pavement surfaces", Applied Mathematical Modeling, Vol. 26, 2002, pp635-652

32. S. Lu, "Spectral analysis and parametric study of stochastic pavement loads", Journal of Engineering Mechanics, Vol.128, March, 2002, pp318-327.

33. G. Rinaldi, M. Packirisamy, I. Stiharu, "Optical MEMS based Bimorph for Thermal Sensing", SPIE conference Photonics North 2004: Fiber Optic Sensors, Ottawa, Canada, Sep. 27-29, 2004.

34. N. Maluf, "An Introduction to Microelectromechanical Systems Engineering", Artech House, 2000.

35. S. D. Senturia, "Microsystem design", Kluwer Academic Publishers, 2001.